*Cerebral Cortex*, March 2019;29: 1305–1327

**doi: 10.1093/cercor/bhy245**
Advance Access Publication Date: 15 December 2018
Original Article



ORIGINAL ARTICLE

# Cytoarchitectonic segregation of human posterior intraparietal and adjacent parieto-occipital sulcus and its relation to visuomotor and cognitive functions

Monika Richter[1], Katrin Amunts[1,2,3], Hartmut Mohlberg[2], Sebastian Bludau[2], Simon B. Eickhoff[4,5], Karl Zilles[2,3,6] and Svenja Caspers[1,2,3]

[1]C. and O. Vogt Institute for Brain Research, Heinrich-Heine-University Düsseldorf, 40001 Düsseldorf, Germany, [2]Institute of Neuroscience and Medicine (INM-1), Research Centre Jülich, 52425 Jülich, Germany, [3]JARA-BRAIN, Jülich-Aachen Research Alliance, 52425 Jülich, Germany, [4]Institute of Neuroscience and Medicine, Brain & Behaviour (INM-7), Research Centre Jülich, 52425 Jülich, Germany, [5]Institute for Systems Neuroscience, Medical Faculty, Heinrich Heine University Düsseldorf, 40001 Düsseldorf, Germany and [6]Department of Psychiatry, Psychotherapy and Psychosomatics, RWTH Aachen University, 52062 Aachen, Germany

Address correspondence to Prof. Dr Svenja Caspers, C. and O. Vogt Institute for Brain Research, Heinrich-Heine-University Düsseldorf, 40001 Düsseldorf, Germany. Email: svenja.caspers@hhu.de.

## Abstract

Human posterior intraparietal sulcus (pIPS) and adjacent posterior wall of parieto-occipital sulcus (POS) are functionally diverse, serving higher motor, visual and cognitive functions. Its microstructural basis, though, is still largely unknown. A similar or even more pronounced architectonical complexity, as described in monkeys, could be assumed. We cytoarchitectonically mapped the pIPS/POS in 10 human postmortem brains using an observer-independent, quantitative parcellation. 3D-probability maps were generated within MNI reference space and used for functional decoding and meta-analytic coactivation modeling based on the BrainMap database to decode the general structural–functional organization of the areas. Seven cytoarchitectonically distinct areas were identified: five within human pIPS, three on its lateral (hIP4-6) and two on its medial wall (hIP7-8); and two (hPO1, hOc6) in POS. Mediocaudal areas (hIP7, hPO1) were predominantly involved in visual processing, whereas laterorostral areas (hIP4-6, 8) were associated with higher cognitive functions, e.g. counting. This shift was mirrored by systematic changes in connectivity, from temporo-occipital to premotor and prefrontal cortex, and in cytoarchitecture, from prominent Layer IIIc pyramidal cells to homogeneous neuronal distribution. This architectonical mosaic within human pIPS/POS represents a structural basis of its functional and connectional heterogeneity. The new 3D-maps of the areas enable dedicated assessments of structure–function relationships.

**Key words:** cytoarchitecture, human brain mapping, intraparietal sulcus (IPS), meta-analysis, parieto-occipital sulcus (POS)

## Introduction

The most prominent anatomical landmark of the human posterior parietal cortex (PPC) is the IPS. It subdivides the PPC into superior (SPL) and inferior (IPL) parietal lobules, whereupon its sulcal pattern varies considerably among individuals (Ono et al. 1990; Ebeling and Steinmetz 1995; Choi et al. 2006; Zlatkina and Petrides 2014). At the parieto-occipital transition, the posterior part of IPS (pIPS) approaches the POS, from which it is typically separated by a gyral passage (Zlatkina and Petrides 2014). The POS separates the PPC (anterior wall of POS) from the occipital lobe (posterior wall of POS) and is typically a continuous sulcus (Ono et al. 1990; Malikovic et al. 2012).

Focusing on the posterior part of IPS (pIPS) and adjacent posterior wall of POS in humans, a differential functional involvement in a variety of visuomotor and cognitive functions has been reported (for review, see e.g. Culham and Kanwisher 2001; Binkofski et al. 2015). Among visuomotor functions, human pIPS and posterior wall of POS are involved in the control of arm and eye movements (Kertzman et al. 1997; Corbetta et al. 1998; Berman et al. 1999; Petit and Haxby 1999; Astafiev et al. 2003; Schluppeck et al. 2005; Konen and Kastner 2008a; Konen et al. 2013). Furthermore, regions within human pIPS and posterior wall of POS are activated by tasks requiring attention (Corbetta et al. 1998; Coull and Frith 1998; Corbetta and Shulman 2002; Silver et al. 2005; Schluppeck et al. 2005, 2006; Uncapher et al. 2011; Rosen et al. 2015), and working memory (Coull and Frith 1998; LaBar et al. 1999; Pessoa et al. 2002; Offen et al. 2010; Barton and Brewer 2013; Raabe et al. 2013; Bray et al. 2015). Human pIPS is additionally involved in spatial cognition (Colby and Goldberg 1999; Husain and Nachev 2007; Sack 2009), as well as processing of motion (Culham et al. 1998; Shulman et al. 1999; Sunaert et al. 1999; Konen and Kastner 2008a), shape of visual objects (Denys et al. 2004; Xu 2008; Konen and Kastner 2008b; Durand et al. 2009; Bettencourt and Xu 2016), and numbers (Dehaene et al. 2003, 1998; Nieder 2005; Dehaene 2009).

Furthermore, several topographically-organized areas have been identified along the anterior–posterior axis of the IPS, defined using visuotopic mapping in memory-guided saccade tasks (Silver et al. 2005; Swisher et al. 2007; Konen and Kastner 2008a; Silver and Kastner 2009). Here, pIPS showed higher connectivity to early and higher visual regions, anterior IPS had stronger connections to prefrontal regions (Uddin et al. 2010; Mars et al. 2011; Greenberg et al. 2012; Bray et al. 2013).

Such an enormous functional diversity raises the question of its structural correlates. Evidence of a structure–function relationship could be derived from studies in monkeys. Microstructural, electrophysiological, and functional analyses revealed a subdivision of monkey pIPS and posterior wall of POS into several distinct areas, named after their topographical position: e.g. lateral (LIP), posterior (PIP), and caudal (CIP) intraparietal area in the pIPS, as well as V6 and V6A in the the POS (Seltzer and Pandya 1986, 1980; Colby et al. 1988; Andersen et al. 1990; Felleman and van Essen 1991; Cavada et al. 2000; Lewis and van Essen 2000; Galletti et al. 2003; Gamberini et al. 2015). Using single-unit recordings and functional magnetic resonance imaging (fMRI) studies in alert monkeys, different visuomotor functions could be associated with distinct microstructurally defined areas, with shifts of functional involvement along an anterior–posterior as well as a medio-lateral axis with regard to visual perceptive, attentional, or sensorimotor functions (Culham and Kanwisher 2001; Orban et al. 2006, 2004; Grefkes and Fink 2005; Orban 2016).

While there is ample evidence on distinct structure–function relationships in monkey pIPS and POS, linking the functional heterogeneity of human pIPS and adjacent posterior wall of POS to its structural underpinnings could hardly be established until now, as detailed anatomical maps were not available. Structural atlases in humans (Fig. 1) comprising a parcellation of this brain region are rare and often of limited use for direct comparison with modern functional neuroimaging data (Zilles and Amunts 2010; Amunts and Zilles 2015). In the most widely used brain map of Brodmann (1909; Fig. 1A), which still influences the present idea of the microstructural organization of the human cortex, both sulci were not further analyzed landmarks within the PPC and adjacent occipital cortex. A cytoarchitectonic parcellation of human IPS based on a single hemisphere was proposed by Gerhardt (1940), resulting in 15 areas around and within the IPS (Fig. 1B). This observation still awaits independent confirmation, being one of the reasons why its impact for understanding functional neuroimaging findings has been marginal. Furthermore, the interindividual variability of the sulcal pattern of IPS and POS was not accounted for in classical cytoarchitectonic maps either. Within the anterior part of the human IPS (aIPS), three cytoarchitectonic areas were identified, using the same observer-independent, quantitative mapping approach as applied in the present study. Two areas were found on the lateral bank and adjacent bottom of aIPS (hIP1, hIP2; Choi et al. 2006), and one on the medial wall (hIP3; Scheperjans, Eickhoff et al. 2008; Scheperjans, Hermann et al. 2008).

To find a respective microstructural basis for the functional diversity of human pIPS and adjacent posterior wall of POS, the cytoarchitecture of this region was mapped in the present study using an observer-independent, statistically testable quantitative mapping method. The resulting cytoarchitectonic maps of human pIPS and posterior wall of POS consider interindividual variability and were registered in the widely used MNI reference space, enabling a direct comparison with functional imaging data. Using quantitative meta-analysis based on the BrainMap database (Eickhoff et al. 2009, 2012), the cytoarchitectonically defined areas were used as seed regions to reveal overall functional network integration of these areas as a starting point for future dedicated assessments on structure–function relationships in this region.

## Material and Methods

### Histological Processing and 3D-Reconstruction of Postmortem Brains

Ten human postmortem brains (five male, five female) were cytoarchitectonically analyzed (Table 1). They were provided by the body donor program of the Anatomical Institute of the University of Düsseldorf, Germany, and comply with the requirements of the local Ethics Committee. Except for one brain with basal ganglia infarction, no other donor showed a history of psychiatric or neurological diseases. After removing the brains from the skull within the first 24 h postmortem, the brains were fixed in 4% formalin or Bodian's fixative for at least 6 months. Prior to histological processing, an MRI scan using a T1-weighted structural 3D FLASH sequence (flip angle = 40°, repetition time = 40 ms, echo time = 5 ms) on a 1.5-T Siemens scanner (Erlangen, Germany) was obtained for each fixed brain, serving as a reference undistorted by histological procedures for subsequent 3D-reconstruction. Histological processing included dehydrating in a rising alcohol series, embedding in paraffin, serial cutting into coronal sections of 20 µm thickness by using a large-scale microtome, mounting of every 15th

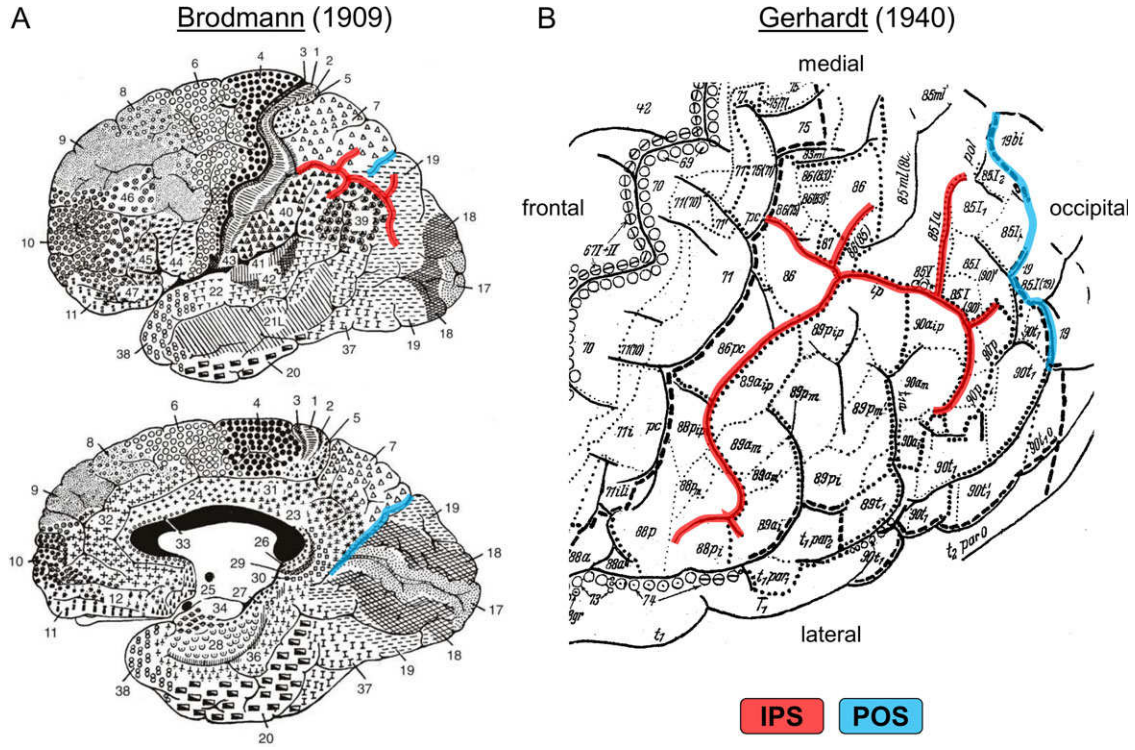


**Figure 1.** Classical cytoarchitectonic human brain maps by (A) Brodmann (1909), lateral and medial view; and (B) Gerhardt, dorsal view (1940). The intraparietal sulcus (IPS) and adjacent parieto-occipital sulcus (POS) are marked in red and blue, respectively.

**Table 1** Ten human post mortem brains used for cytoarchitectonic analysis from the brain collection of the C. and O. Vogt Institute for Brain Research, University of Düsseldorf, Germany.

| Brain-code | Age [years] | Gender | Brain weight (fresh) [g] | Cause of death |
|---|---|---|---|---|
| 2 | 56 | Male | 1270 | Rectal carcinoma |
| 4 | 75 | Male | 1349 | Necrotized glomerulonephritis |
| 5 | 59 | Female | 1142 | Cardiorespiratory insufficiency |
| 7 | 37 | Male | 1437 | Acute heart failure |
| 8 | 72 | Female | 1216 | Renal failure |
| 9 | 79 | Female | 1110 | Heart failure, infarction in the basal ganglia |
| 10 | 85 | Female | 1046 | Mesenteric infarction |
| 12 | 43 | Female | 1198 | Lung embolism, cor pulmonale |
| 13 | 39 | Male | 1234 | Drowning |
| 20 | 65 | Male | 1392 | Cardiorespiratory insufficiency, carcinoma of the prostate |

section on glass slides, and staining for cell bodies with a modified silver stain (Merker 1983). Every 60th histological section was used for cytoarchitectonic analyses and digitized in a flatbed scanner. During the cutting process, blockface images were obtained using a CCD camera (XC-75, Sony, Japan, image matrix = 256 × 256 pixels, 8 bit gray value resolution). Integrating the undistorted MR-images with the blockface and digitized images after histological processing, the postmortem brains were 3D-reconstructed (Amunts et al. 2000).

## Observer-Independent Detection of Cortical Borders

Based on observer-independent and statistically testable criteria, cytoarchitectonic areas were delineated (Schleicher et al. 2009, 1999). Briefly, a rectangular region of interest (ROI) was defined in images of histological sections covering the pIPS caudal to hIP1-3 and the adjacent posterior wall of POS (Fig. 2A). The ROIs were scanned in a mosaic-like pattern with a high-resolution CCD camera (AxioCam MRm, Zeiss, Germany) attached to a computer-controlled microscope (Axio Observer. Z1, Zeiss, Germany). Using in-house software implemented in Matlab (The MathWorks, Inc., Natick, MA, USA), digitized ROIs were converted into gray level index (GLI) images (Schleicher et al. 1999). The GLI reflects the volume fraction of stained cell bodies (Wree et al. 1982; Schleicher and Zilles 1990; Schleicher et al. 1999) within a measuring field of 17 μm × 17 μm, ranging from 0% (only neuropil) to 100% (only cell bodies). In each GLI image, equidistant GLI profiles were extracted as traverses perpendicular to the cortical layers between interactively defined outer (between layer I and II) and inner (between layer VI and the white matter) contour lines (Fig. 2B; Schleicher et al. 1999, 2000, 2005). The GLI profiles along these traverses represented laminar changes in volume density of cell bodies, thus reflecting cortical cytoarchitecture (Schleicher et al. 2009). Variations

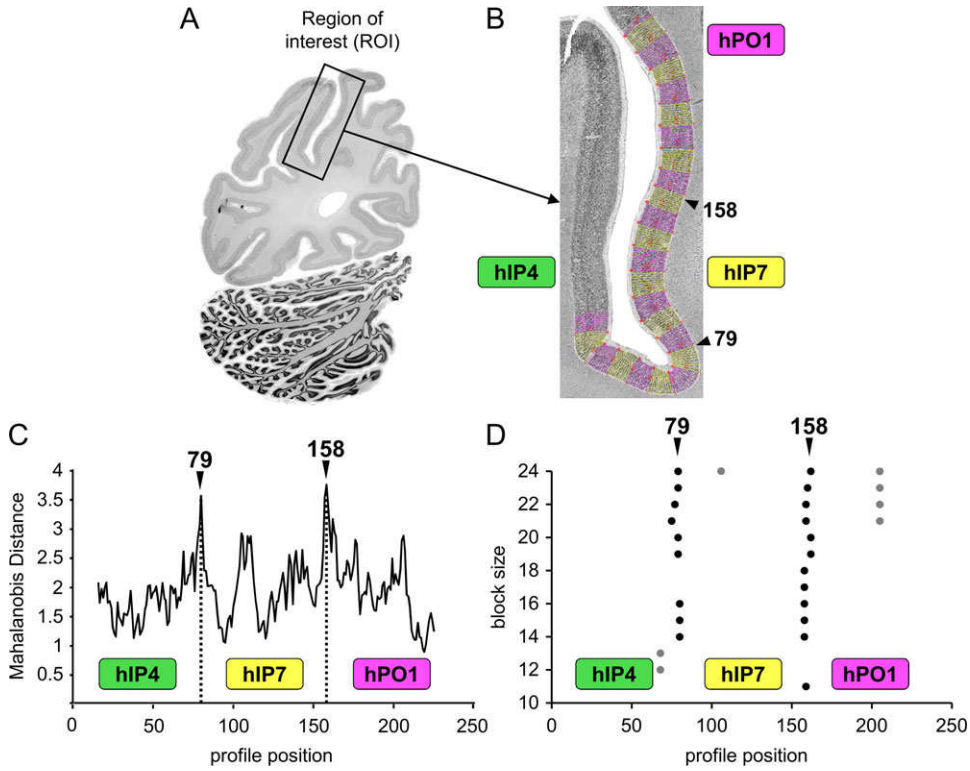


**Figure 2.** Example of the detection of cytoarchitectonic borders within the pIPS and posterior wall of POS using an observer-independent mapping algorithm (Schleicher et al. 1999). (A) Microscopical definition of a region of interest (ROI)—marked with a box—within a histological section of the left hemisphere. The ROI was digitized and converted into a GLI image. (B) Converted GLI image of this ROI, superimposed with the interactively traced outer and inner contour lines (white lines) and equidistant traverses, running perpendicular to the cortical layers. Color changes between yellow and pink after every 10th traverse. Along these traverses GLI profiles were extracted. (C) The Mahalanobis distance functions (ordinate) plotted against profile positions (abscissa) for a particular block size b. Significant maxima of the Mahalanobis distance function refer to profile positions with potential borders between two cytoarchitectonically different cortical areas. In this example, the Mahalanobis distance reaches significant local maxima at profile positions 79 and 158. (D) Profile positions (abscissa) of significant maxima of the Mahalanobis distance functions (points) plotted for different block sizes (ordinate) $b = 10$ (bottom) to 24 (top). For most of the block sizes $b$, the Mahalanobis distance function reaches significant maxima at or adjacent to profile positions 79 and 158, corresponding to the border between hIP4 and hIP7, and between hIP7 and hPO1, respectively.

in cortical thickness were compensated for by normalizing the length of each profile to 100% (= normalized cortical thickness) via linear interpolation. To characterize the GLI profile curve a feature vector with ten elements was calculated, containing five features (mean GLI value, mean of cortical depth, standard deviation of the mean GLI, skewness, kurtosis) from the original GLI profile and the corresponding five features from its differential quotient (Schleicher et al. 1999). To increase signal-to-noise GLI profiles were summed up to blocks of 10–24 GLI profiles. Blocks for each block size were systematically moved along the cortical ribbon using a sliding window technique. To quantify differences in shape of mean GLI profiles between neighboring blocks, the Mahalanobis distance (Mahalanobis et al. 1949) was calculated as a measure for similarity or dissimilarity between the profiles. A significant maximum of the Mahalanobis distance function indicated a cytoarchitectonical border (Fig. 2C), and was tested for statistical significance using a Hotelling's T2 test ($P < 0.01$, Bonferroni-corrected for multiple comparisons; Schleicher et al. 1999). A peak was accepted as a cytoarchitectonical border between cortical areas, if the Mahalanobis distance showed significant maxima for different block sizes ($b = 10$–24) at comparable profile positions (Fig. 2D), and if this border was found at comparable position along the cortical ribbon in adjacent sections. Finally, each automatically and observer-independently detected border was verified by microscopic inspection of the sections to exclude detection of "artificial borders" caused by, e.g. larger blood vessels, or wrinkles or other artifacts caused during mounting and staining of the sections, which would lead to artificial distortions of profile curves.

### 3D Cytoarchitectonic Probability Maps in Stereotaxic Space

Delineations of all areas in pIPS and posterior wall of POS were manually transferred onto corresponding digitized sections using in-house software, and 3D-reconstructed in each post-mortem brain. The brains and delineated areas were registered to the T1-weighted single-subject template brain (Colin27; Evans et al. 1992) of the standard reference space of the Montreal Neurological Institute (MNI) via combination of linear affine and non-linear elastic transformations (Hömke 2006). Data aligned to the Colin27 brain in original MNI space were then shifted linearly by 4 mm in the y-axis and 5 mm in the z-axis to the "anatomical MNI space". This procedure resulted in a shift of the origin of the coordinate system to the anterior commissure (Amunts et al. 2005). Note that this is not equivalent to transforming data to the Talairach space as this requires a non-linear transformation (e.g. Lacadie et al. 2008). By superimposing each identified region of all 10 brains in the MNI single-subject brain (Colin27), 3D continuous probability maps were generated for each area. These probability maps assigned

each voxel of the reference brain the relative frequency with which a cortical area was located at a particular position in the reference space across all 10 postmortem brains, represented in a continuous map (e.g. Lorenz et al. 2017). The probability maps thus quantified interindividual anatomical variability of a cortical area in the reference space, continuously ranging from 0 to 100%. This variability led to spatial overlap of neighboring probability maps of pIPS and posterior wall of POS areas, which prevented unambiguous assignment of each voxel to a particular area. Therefore, continuous non-overlapping maximum probability maps (MPMs) were calculated by assigning each voxel of the reference brain to the cortical area with the highest probability in this voxel (Eickhoff et al. 2006). If two or more areas show equally high probabilities at a specific voxel, this voxel was assigned to the cortical area with the higher average probability in the neighboring voxels.

## Volumetry

The volume of each identified area was calculated separately for each hemisphere, based on area measurements in the digitized histological sections (for details, see Amunts et al. 2007). The volume $V$ [$mm^3$] is a function of the distance $s$ between analyzed sections (i.e. every 60th section of the continuous series of sections was analyzed, therefore $s = 60 \times 20\,\mu m = 1.2\,mm$), the pixel size ($\Delta x = \Delta y = 21.16\,\mu m$), the shrinkage factor ($F$) of each individual brain caused by the histological processing, and the number of pixels ($N$) of the cortical area in the section number $i$:

$$V = s \times \Delta x \times \Delta y \times F \times \sum N_i$$

For each brain, the individual shrinkage factor $F$ was calculated as the ratio between its fresh volume and its volume after histological processing (Amunts et al. 2007). The corrected mean volumes of all areas were statistically analyzed for sex and hemispheric differences, as well as the interaction between hemispheric and gender differences by using pairwise permutation tests in Matlab (Bludau et al. 2014). For testing these differences against the null-hypothesis of side exchangeability, each hemisphere was randomly reassigned to one of two possible groups (male/female and left/right, respectively), and the differences between those randomly assembled groups were calculated anew. This procedure was repeated a million times. Sex or hemispheric differences were considered significant, if they were larger than 95% of the values under the null-hypothesis ($P < 0.05$; False Discovery Rate corrected for multiple comparisons).

## Hierarchical Cluster Analysis and Analysis of Multidimensional Scaling of Cytoarchitectonic Features

Using Matlab, the degree of similarities or dissimilarities in cytoarchitecture between pIPS and posterior wall of POS areas was quantified by performing a hierarchical cluster and a multidimensional scaling analysis. For each area, a block of 15 GLI profiles was selected in each of three selected sections without apparent artifacts or oblique sectioned segments of the cortex. From these 45 GLI profiles for each area in each hemisphere and brain, mean GLI profiles and corresponding feature vectors were computed, representing a quantification of the underlying cytoarchitecture. In the hierarchical cluster analysis, the clustering of these feature vectors was performed using the Euclidean distance and the Ward linkage method (Ward 1963) and visualized as a hierarchical dendrogram. Areas with a high degree of cytoarchitectonic similarities were merged to one cluster, reflected by low Euclidean distance in between. The more the value of Euclidean distance increased, the more dissimilar areas were in terms of their cytoarchitecture. A multidimensional scaling analysis was used to reduce data complexity and visualize the degree of similarities or dissimilarities of each pIPS and posterior wall of POS area in a 2D distance matrix, together with the confidence intervals of 95%.

## Quantitative Meta-Analysis

Using the online database BrainMap (http://brainmap.org; Fox and Lancaster 2002; Laird et al. 2005), a quantitative coordinate-based meta-analysis was performed, comprising three parts: (1) functional decoding of each area of pIPS and posterior wall of POS for functional characterization, (2) functional connectivity analyses by obtaining coactivation maps, and (3) conjunction and contrast analyses to statistically test for commonalities and differences in coactivation patterns. The aim of this analysis was to reveal overall organizational principles of functional involvement and brain network integration of the identified areas in pIPS and posterior wall of POS based on a multitude of different functional imaging studies, as a starting point for future dedicated assessments of specific structure–function relationships in this region. From the BrainMap database, 3D activation coordinates in a standard reference space from published functional neuroimaging experiments as well as corresponding meta-data (Laird et al. 2009, Riedel et al. 2013) were considered for the present analyses. The MPMs of each area in pIPS and posterior wall of POS within the MNI152 reference space were used as seed regions (after transformation from the Colin27 space), separately for left and right hemisphere, resulting in 14 seed regions in total. Based on these MPMs, the BrainMap database was searched for fMRI and positron emission tomography (PET) studies in healthy subjects, which showed at least one focus of activation within the defined seed regions. These requirements restricted the multitude of neuroimaging experiments within the BrainMap database to 3100 eligible experiments (at the time of analysis: August 2016), which were used for this study.

For the functional decoding of each area in pIPS and posterior wall of POS area, the meta-data "Behavioral domains" and "Paradigm classes" were used. Behavioral domains describe the mental processes isolated by the experimental contrast, whereas paradigm classes describe the experimental tasks that were used in the experiment (see http://www.brainmap.org/taxonomy/). For each seed region, the frequency of behavioral domain and paradigm class "hits" was plotted against its likelihood across the entire database (Eickhoff et al. 2011). Only if the behavioral domains or paradigm classes were significantly overrepresented in a given seed region, for both the forward inference and the reverse inference, they were included into the functional profile of the seed. Forward inference P(Activation | behavioral domain *or* paradigm class) reflected the probability of finding activation in a seed region given a predefined behavioral domain or paradigm classes, whereas reverse inference P(behavioral domain or paradigm class | Activation) indicated the probability of being involved in a particular behavioral domain or paradigm classes given activation in a seed region. Significance was tested using a binomial test ($P < 0.05$, Bonferroni-corrected for multiple comparisons; Laird et al. 2009; Eickhoff et al. 2011).

Whole-brain coactivation maps were generated to analyze the functional connectivity of each area in pIPS and posterior wall of POS area by using meta-analytic connectivity modeling (MACM) and the modified Activation Likelihood Estimation (ALE) algorithm (Turkeltaub et al. 2012, 2002; Eickhoff et al. 2016, 2012, 2009; Laird et al. 2009; Robinson et al. 2010). Using the ALE algorithm, the reported coordinates from the eligible functional studies were considered as spatial Gaussian probability distributions centered at the coordinates (Eickhoff et al. 2009). For each experiment, modeled activation maps were calculated by combining all probabilities for each voxel. The union of these maps across all experiments provided voxel-wise ALE scores, reflecting convergence of functional activation foci across subjects. To test for "true" convergence, these ALE scores were tested against an empirical null-hypothesis of random spatial association of activation foci using permutation tests ($P < 0.05$, family wise error (FWE)-corrected for multiple comparisons) (Eickhoff et al. 2016, 2012; Turkeltaub et al. 2012). The final ALE maps reflected consistent coactivation across studies with the seed region. Notably, highest convergence was observed in each seed, as functional experiments were selected based on their activation in this seed. The term functional connectivity will be used throughout the manuscript in the context of coactivation patterns according to the MACM approach.

To investigate commonalities and differences in coactivation patterns of the seed regions in pIPS and posterior wall of POS, conjunction and contrast analyses were performed using the minimum statistic (Nichols et al. 2005). Contrast analyses were performed by voxel-wise calculation of differences between ALE maps of individual MACM analyses (Eickhoff et al. 2011). Contrast analyses were tested for significance against an empirical null distribution (random assignment of experiments to either seed region) using a permutation test with 10 000 repetitions. Results were considered significant if showing up in a map thresholded at a posterior probability of $P > 0.95$. For further information, see Eickhoff et al. (2016, 2012, 2009).

## Results

### Topography of Seven Cytoarchitectonically Distinct Areas in pIPS and Posterior Wall of POS

Seven cytoarchitectonically distinct areas were identified within human pIPS and posterior wall of POS (Fig. 3A). Areas hIP4-8 were localized within pIPS, areas hPO1 and hOc6 on the posterior wall of POS. High-resolution depictions of all cytoarchitectonic areas (Figs 5–8) and their borders are available as supplementary high-resolution figures for download (Supplementary Figs S1–S10).

Topographically, these seven areas covered the pIPS and adjacent posterior wall of POS in between surrounding cytoarchitectonic areas of caudal inferior parietal lobule (IPL: areas PGa, PGp; Caspers et al. 2008, 2006) and superior parietal lobule (SPL: areas 7A, 7P, 7M; Scheperjans, Eickhoff et al. 2008; Scheperjans, Hermann et al. 2008), as well as anterior IPS (areas hIP1, hIP2, hIP3; Choi et al. 2006; Scheperjans, Eickhoff et al. 2008; Scheperjans, Hermann et al. 2008) and dorsal occipital cortex (areas hOc2, hOc3d/V3d, hOc4d/V3A; Amunts et al. 2000; Kujovic et al. 2013) (Fig. 3A,B). From caudal to rostral, areas hIP4-6 covered the lateral wall of pIPS, adjoining IPL areas PGa and PGp, with hIP6 abutting anterior IPS areas hIP1 and hIP3 rostrally. Since the areas hIP4-6 partially encroach on the medial wall of pIPS, they bordered medial pIPS areas hIP7 and hIP8. Caudal medial pIPS area hIP7 had common borders with area hPO1, whereas rostral medial pIPS area hIP8 bordered hPO1 and SPL areas 7P and 7A. Area hPO1, located at the junction between pIPS and posterior wall of POS, bordered occipital area hOc4d/V3A. Area hOc6 was found in the depth of posterior wall of POS in the occipital lobe, abutting occipital areas hOc3d/V3d and hOc2/V2. Despite substantial interindividual variability in sulcal morphology of pIPS and POS, this topographical arrangement of the seven areas in the pIPS and posterior wall of POS was consistently found across all ten brains studied: Areas hIP4, hIP5, and hIP6 were always found on the lateral wall of pIPS, and areas hIP7 and hIP8 always on the medial wall of pIPS, whereas hPO1 and hOC6 were always located on the posterior POS wall, indicating a consistent relation between sulci and cytoarchitectonic areas. Local peculiarities in topography of the areas in case the pIPS was a continuous or subdivided sulcus (with a rostral superficial and caudal deep branch) are exemplarily shown in Fig. 4. In contrast, the POS appeared as one continuous sulcus, with the occipital lobe forming its posterior and the superior parietal lobule forming its anterior wall. POS and pIPS were separated by a gyrus, whose width varied among individual brains.

### Cytoarchitectonic Characteristics of Areas in the pIPS and Posterior Wall of POS

#### *Lateral Bank of pIPS: Cytoarchitecture of Areas hIP4-6*

The lateral bank of pIPS was covered by cytoarchitectonic areas hIP4-6, which differ between each other mainly in layers III and layer V with regard to their cell packing density and size as well as their width (Fig. 5A, Supplementary Fig. S1). From caudal to rostral, hIP4 was replaced by hIP5 (Fig. 5B, Supplementary Fig. S2), and hIP5 was displaced by hIP6 (Fig. 5C, Supplementary Fig. S3), pushing it towards the fundus of the sulcus.

Rostral area ***hIP6*** showed high cell packing density in all layers, a narrower Layer III and a broader Layer VI in comparison to the other lateral pIPS areas. Layer III was clearly delineated from cell-dense Layer II, containing columns of pyramidal cells with slight superficial-to-deep increase in size. With Layer IV being very thin and less dense (local minimum of the mean GLI profile; Fig. 5A, marked with a red arrow), Layer V was clearly marked by evenly distributed pyramidal cells with diminishing size from Layer Va to Vb, but being larger than those in Layer IIIc and intermingling with cell dense Layer VI.

In contrast to area hIP6, ***hIP5*** had lower cell density across all layers, a broader Layer III with evenly distributed pyramidal cells, a sparsely developed Layer IV, and a two-parted Layer V with a cell-dense upper and cell-sparse lower part (Fig. 5C). Layer VI was more discrete, with a sharp border to the white matter.

Contrarily, caudal area ***hIP4*** was characterized by the widest Layer III, which was two-parted, and the thinnest Layer V, which could not be subdivided into sublayers. The bipartition of Layer III was reflected by an abrupt change from a cell-sparse superficial part with small, evenly distributed pyramidal cells to a cell dense deep part with larger pyramids in columnar arrangement. Thin Layer IV was clearly delimited from Layer III (local minimum of the mean GLI profile; Fig. 5A, marked with a red arrow), but interrupted by strands of large pyramidal cells from thin and homogeneous Layer V.

Further cytoarchitectonic borders between lateral pIPS and IPL areas PGa, PGp or medial anterior IPS area hIP3 were depicted in the papers of Caspers et al. (2006) or Scheperjans, Hermann et al. (2008).

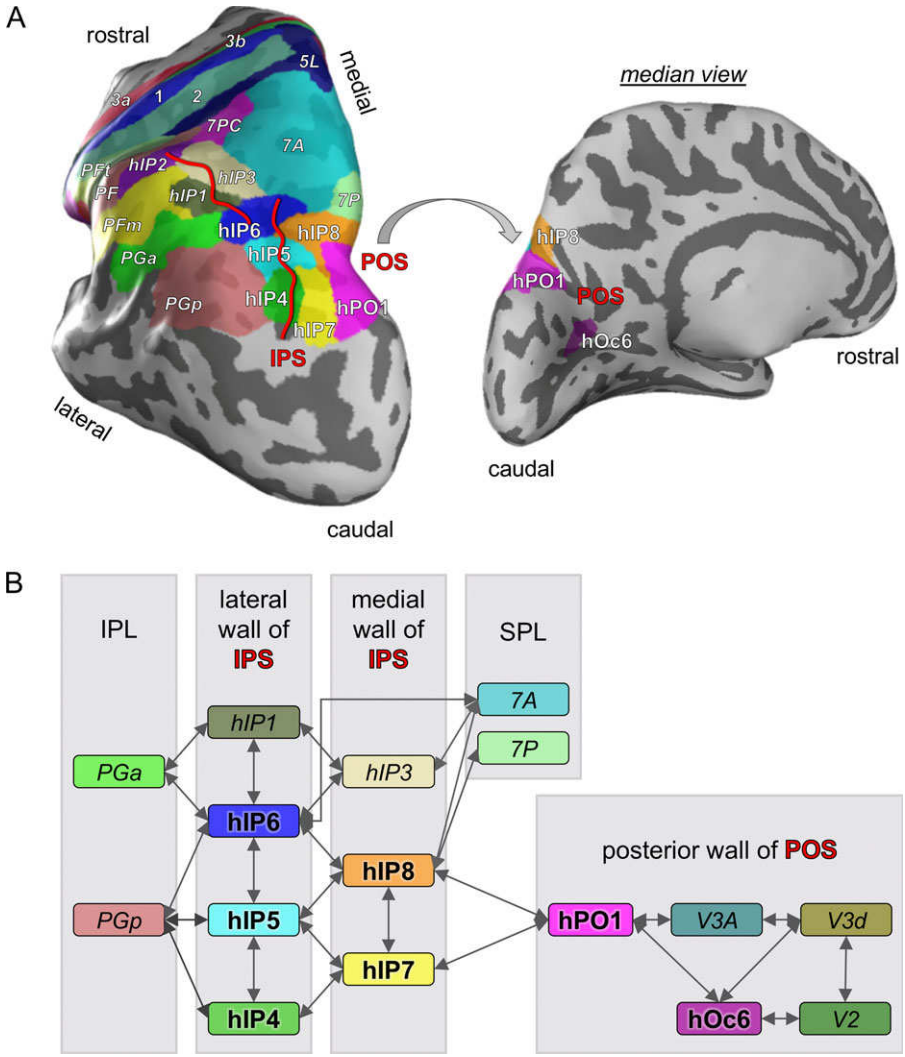


**Figure 3.** Topography of seven cytoarchitectonically distinct areas within human pIPS and adjacent posterior wall of POS, in relation to their surroundings. (A) Areas of pIPS and adjacent posterior wall of POS (normal large font) as maximum probability maps overlaid onto an inflated surface of the left hemisphere of the MNI single-subject (Colin27) brain, with previously published maps of inferior parietal lobule (IPL; Caspers et al. 2006, 2008: areas PFt, PF, PFm, PGa, PGp), superior parietal lobule (SPL; Scheperjans, Eickhoff et al. 2008; Scheperjans, Hermann et al. 2008: areas 5L, 7PC, 7A, 7P), primary somatosensory cortex (Geyer et al. 2000, 1999: areas 3a, 3b, 1, 2; Grefkes et al. 2001), anterior IPS (Choi et al. 2006, Scheperjans, Eickhoff et al. 2008; Scheperjans, Hermann et al. 2008: areas hIP1, hIP2, hIP3) surrounding them. Major course of the IPS delineated in red. (B) Schematically depicted topographical relationship between areas in pIPS and posterior wall of POS and adjacent parietal and occipital areas. Arrows indicate common borders between the areas on either side of the arrows.

***Medial Bank of pIPS: Cytoarchitecture of Areas hIP7-8***

The medial bank of pIPS was lined with hIP7 and hIP8, from caudal to rostral, until they were replaced by anterior IPS area hIP3 (Scheperjans, Hermann et al. 2008). The major cytoarchitectonic differences between the two medial areas hIP7 and hIP8 were the overall cell density and the cell distribution in Layer V (Fig. 6A, Supplementary Fig. S4).

Caudal area ***hIP7*** appeared very homogeneous, with overall high cell density and blurred transitions between layers. Layer II was wider than in adjacent hIP8 (Fig. 6B, Supplementary Fig. S5) and hIP4 (Fig. 7A, Supplementary Fig. S6). The broad Layer III showed a columnar arrangement of pyramidal cells with pronounced superficial-to-deep increase in cell size and very large pyramids in Layer IIIc spreading into thin and cell-sparse Layer IV (local GLI minimum; Fig. 6A, marked with a red arrow). The latter applied also to the medium-sized pyramidal neurons in Layer V, which continued into similarly structured, cell dense Layer VI, which was broader than in hIP4 (Fig. 7A) and hIP8 (Fig. 6B).

Rostromedial area ***hIP8*** showed similar cytoarchitectonic features as adjacent lateral area hIP5, with overall lower cell density and a bipartite Layer V. Major differences to hIP5 resulted from a broader Layer III and thinner Layer V in hIP8 (Fig. 7B, Supplementary Fig. S7). Particularly an abrupt change in size of pyramidal cells from superficial to deep parts of Layer III as well as a cell-sparse light stripe between Layers IIIc and IV in area hIP8 stood out in comparison with area hIP5 (local GLI minimum; Fig. 6A, marked with a red arrow). Layer Va appeared as a cell-dense dark stripe (local GLI maximum; Fig. 6A, marked with a red star) in contrast to thin Layer IV and cell-sparse Layer Vb, which was again clearly separable from Layer VI.

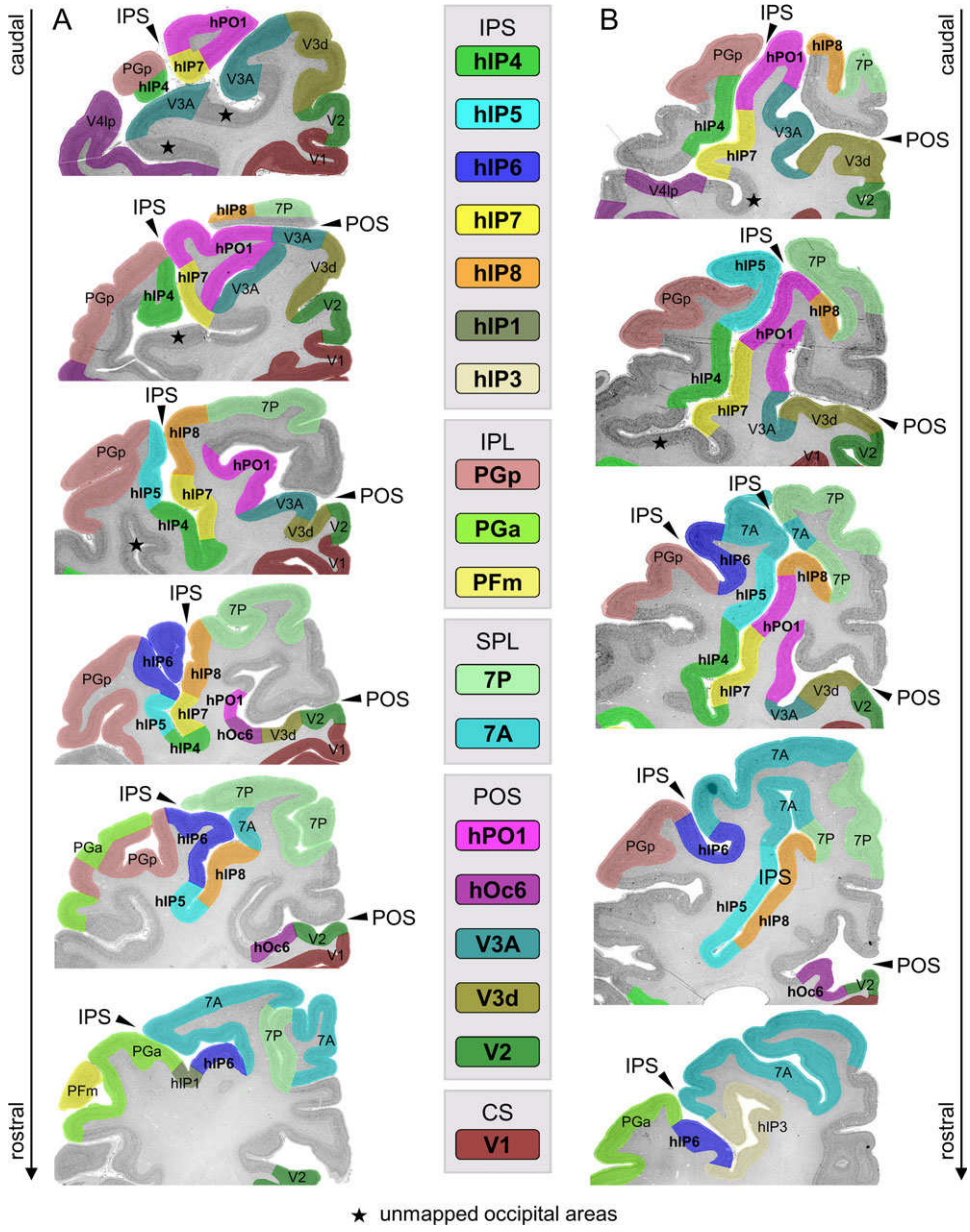


**Figure 4.** Topography of pIPS and posterior wall of POS and surrounding parietal and occipital areas within (A) a continuous IPS and (B) a two-parted IPS, with a rostral superficial and caudal deep branch. The topographical relationship towards neighboring areas of IPL (PGp, PGa, PFm), the SPL (7P, 7A) and occipital areas (V1, V2, hOc3d/V3d, hOc4d/V3A) is also shown. The areas are superimposed on histological sections of two individual post mortem brains used for cytoarchitectonic analyses.

***Posterior Wall of POS: Cytoarchitecture of Areas hPO1, hOc6***

The posterior wall of POS was covered by hPO1 and hOc6, which could be distinguished cytoarchitectonically by homogeneity of Layer III and the width of Layer IV (Fig. 8).

Area ***hPO1*** was characterized by a two-parted Layer III with large pyramidal cells arranged in small groups in its deeper part, reflected in a pronounced local GLI maximum (Fig. 8A: marked with a red arrow, Supplementary Fig. S8). Layer IV was thin and partly interrupted, but clearly separated from Layer III. Layer V was rather homogeneous, with barely detectable sublayers. The border between Layer VI and the white matter was clearly visible. In contrast to medial pIPS area hIP7, which bordered on hPO1 at the junction between pIPS and posterior wall of POS, the size of pyramidal cells in lower Layer IIIc was smaller and Layer V appeared brighter, due to a lower cell density in Layer V (Fig. 8B, Supplementary Fig. S9).

Area ***hOc6*** was located more rostral in ventral aspects of the posterior wall of POS and showed a more homogenous Layer III, a wider Layer IV, and a thinner Layer V than hPO1 (Fig. 8A). Layer II was sharply separated from Layer III, in which pyramidal cells were distributed more homogenously than in hPO1, but still with a visible bipartition. The less dense but thin Layer V contained evenly distributed pyramidal cells, with a few larger ones close to Layer IV. The compact Layer VI had higher cell density, which demarcated it from the white matter. Compared with the occipital area hOc2/V2 (Amunts et al. 2000), the gradient of pyramidal cell size in Layer III was smaller and Layer IV thinner (Fig. 8C, Supplementary Fig. S10).

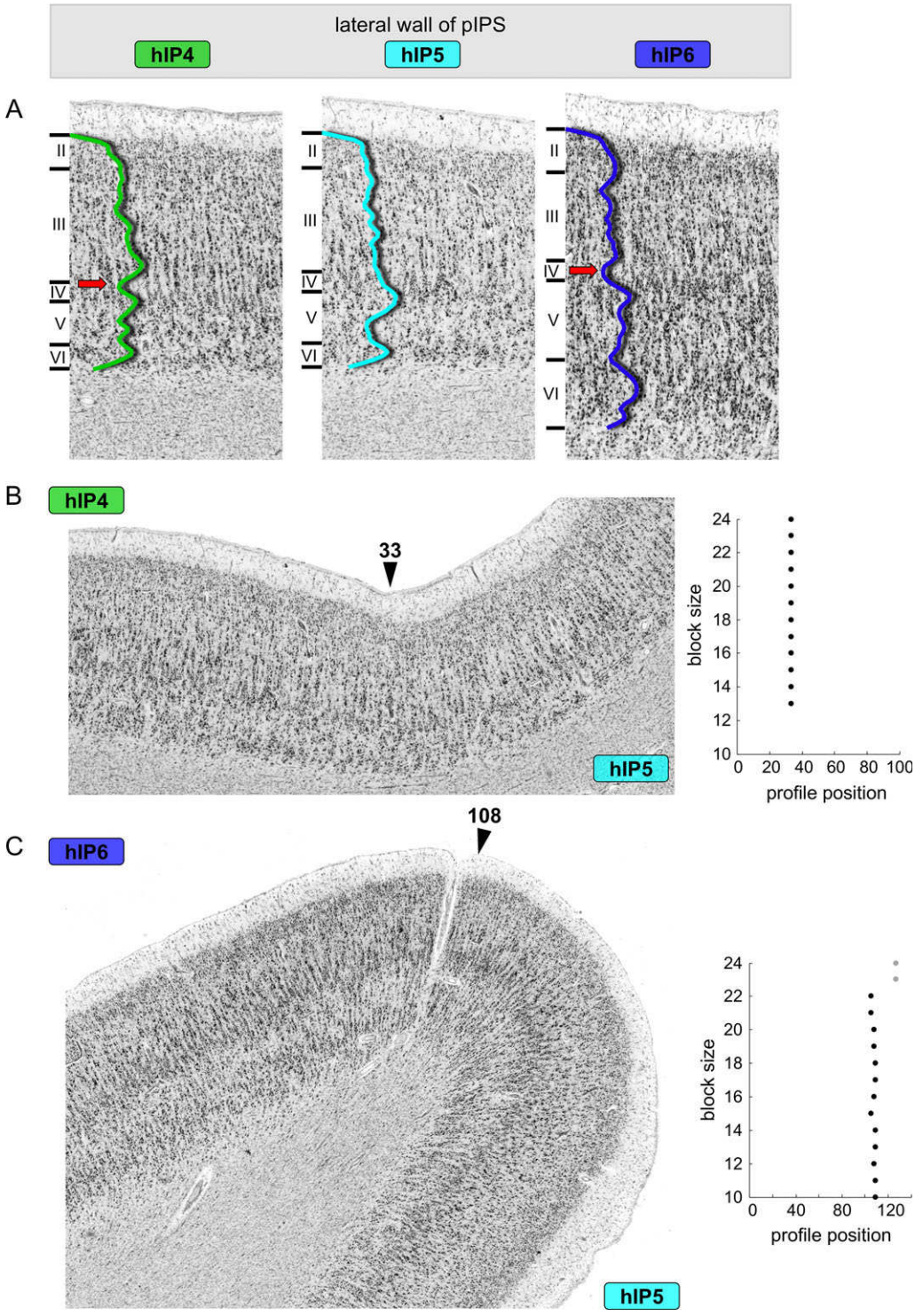


**Figure 5.** Cytoarchitecture of lateral pIPS. (A) Cytoarchitectonic features of lateral pIPS areas hIP4-6 within one investigated brain. Cytoarchitectonic borders on the lateral wall of pIPS between (B) hIP4 and hIP5 at profile position 33 and (C) hIP5 and hIP6 at profile position 108 (marked with black arrows). On the right, the corresponding plots of significant ($P < 0.01$) maxima of the Mahalanobis distance function for different profile block sizes ($b = 10–24$) are depicted. Scale bars according to labeling within the figure.

## Hierarchical Cluster and Multidimensional Scaling Analysis of Cytoarchitectonic Features

The hierarchical cluster-analysis (Fig. 9A) and the multidimensional scaling (MDS) analysis (Fig. 9B) revealed a grouping of the seven areas in pIPS and posterior wall of POS (averaged across left and right hemisphere) into three main clusters: mediocaudal, rostral and lateral. Areas hPO1 and hIP7 were most similar to each other. Both areas were characterized by prominent pyramidal cells in lower Layer IIIc, a local GLI minimum in

position of Layer IV, and a cell dense Layer V with medium-sized pyramidal cells. Together with area hOc6, they formed the mediocaudal cluster, which was distinct from both the rostral and lateral pIPS clusters. MDS analysis additionally visualized this shift across the clusters, as these were mainly separated in the dimension of Score (1). Especially in the MDS analysis of (Fig. 9B), area hOc6 appears as a fringe area, standing out from all other areas, which further supports the notion of a being different from the other areas within pIPS and adjacent posterior wall of POS. Cytoarchitectonic characteristics of the rostral cluster with areas hIP5 and hIP8 were a low overall cell density across all cortical layers, and a two-parted Layer V with a local GLI maximum corresponding to Layer Va. The lateral cluster, consisting of areas hIP4 and hIP6, was characterized by homogeneity across all layers, and a small cleft between Layers IIIc and IV. Overall, the mediocaudal and rostral clusters were more similar to each other as compared with the lateral cluster in terms of cytoarchitecture. Notwithstanding, all pIPS and posterior wall of POS areas show a high degree of similarity, as they are all part of higher-order association cortex, which is particularly evident from considerable intermingling of the individual data points in the MDS analysis (Fig. 9B).

## Probability Maps, Stereotaxic Location, and Volumetry

For each area in pIPS and posterior wall of POS, 3D continuous probability maps were generated in the MNI-Colin27 reference brain to quantify interindividual anatomical variability in their localization and extent. The probability maps of all areas are depicted in Figure 10. The corresponding coordinates of the centers of gravity are shown in Table 2, separately for the left and right hemisphere. The non-overlapping maximum probability maps (MPMs) of the region of pIPS and posterior wall of POS represented the topography and relationships with surrounding parietal and occipital areas (Fig. 3). These cytoarchitectonic maps of all seven cytoarchitectonic areas in pIPS and posterior wall of POS are made publicly available as part of the JuBrain atlas (https://jubrain.fz-juelich.de) and via the Anatomy Toolbox (Eickhoff et al. 2005; http://www.fz-juelich.de/inm/inm-1/DE/Forschung/_docs/SPMAnatomyToolbox/SPMAnatomyToolbox_node.html).

The corrected mean volumes of all areas in pIPS and posterior wall of POS and the corresponding standard deviation of the left and right hemisphere are listed in Table 3. All areas within pIPS (hIP4-8) were about the same size, in contrast to posterior wall of POS area hPO1, which was the biggest, and area hOc6, which was the smallest area. Interindividual variability in volume was most pronounced for area hPO1 and least for area hOc6. The corrected volumes did not differ between the hemispheres nor between the sexes. Additionally, no interaction between hemispheric and gender were found (all $P > 0.05$).

## Quantitative Meta-Analysis

### *Functional Characterization of Each Area in pIPS and Posterior Wall of POS*

The behavioral domains (Fig. 11A) and paradigm classes (Fig. 11B) significantly associated with each area of pIPS and

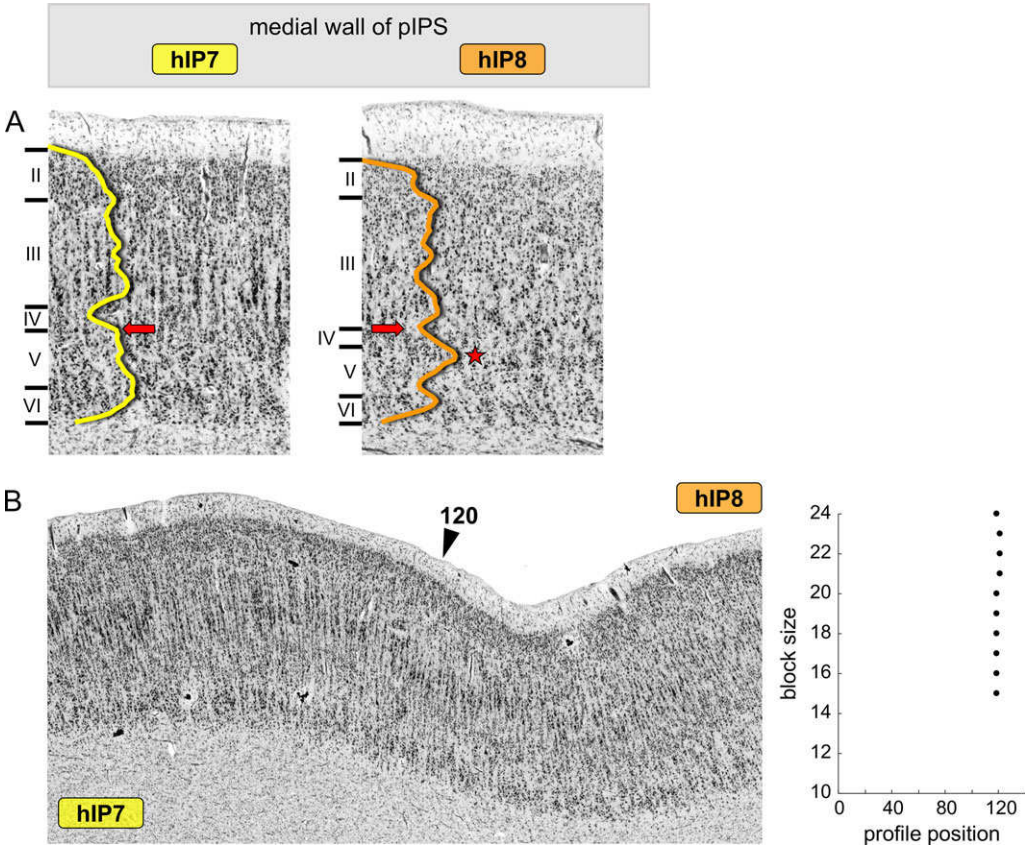


**Figure 6.** Cytoarchitecture of medial pIPS. (A) Cytoarchitectonic features of medial pIPS areas hIP7-8 within one investigated brain. (B) Cytoarchitectonic borders on the medial wall of pIPS between hIP7 and hIP8 at profile position 120 (marked with a black arrow). On the right, the corresponding plot of significant ($P < 0.01$) maxima of the Mahalanobis distance function for different profile block sizes ($b = 10–24$) is depicted. Scale bars according to labeling within the figure.

posterior wall of POS were assessed using the BrainMap database. In this study, all behavioral domains fell into three main categories: cognition, perception and action. All areas in pIPS and posterior wall of POS were involved in spatial cognition, visual perception of motion and shape, working memory, and attention. Compatible with this, all areas were activated during tasks involving mental rotation, visuospatial attention, delayed match to sample, and the Wisconsin card sorting test. Notably, all areas of pIPS and posterior wall of POS in both hemispheres were involved in spatial cognition, while visual perception of motion was more associated with left-sided regions, particularly in rostro-lateral pIPS (areas hIP4-6 and hIP8). Rostral and lateral pIPS (hIP4-6, hIP8) areas were additionally involved in reasoning, language processing and orthography (hIP6), explicit memory (hIP5) and action inhibition (hIP6,8), whereupon caudal area hIP4 was just involved in reasoning. Only hIP5, hIP6, and hIP8 were activated during counting and calculation tasks, visual identification of objects and covert word generation (only hIP5,6). In contrast, mediocaudal areas of pIPS and posterior wall of POS were associated with action observation (hIP7) and visual perception of color (hPO1). Together with hIP4, they were activated during visual tracking of moving targets. The mediocaudal areas and the medial area hIP8 were activated during saccades. No significant association of behavioral domains or paradigm classes listed in the BrainMap database was found for area hOc6.

### *MACM: Conjunction and Contrast Analyses*

The conjunction of coactivation maps of all areas in pIPS and posterior wall of POS, except hOc6, revealed a common network of cortical and subcortical brain regions (Fig. 12A). This bilateral network included the ventral and dorsal premotor cortex (PMC) and the (pre)supplementary motor area (SMA and preSMA). Additional coactivations were found bilaterally in the ventrolateral prefrontal cortex (vlPFC), frontal operculum (FO) and anterior insula, area 44 (Broca's region; Amunts et al. 1999), as well as intraparietal areas. Compared with existing cytoarchitectonic probability maps, the intraparietal activation contained the anterior IPS areas hIP1, hIP2 (Choi et al. 2006), hIP3 (Scheperjans, Eickhoff et al. 2008; Scheperjans, Hermann et al. 2008) and the seed regions within the pIPS. Further significant coactivation of areas of pIPS and posterior wall of POS was found in the dorsal (dOC), ventral (vOC) and lateral occipital cortex (LOC), comprising

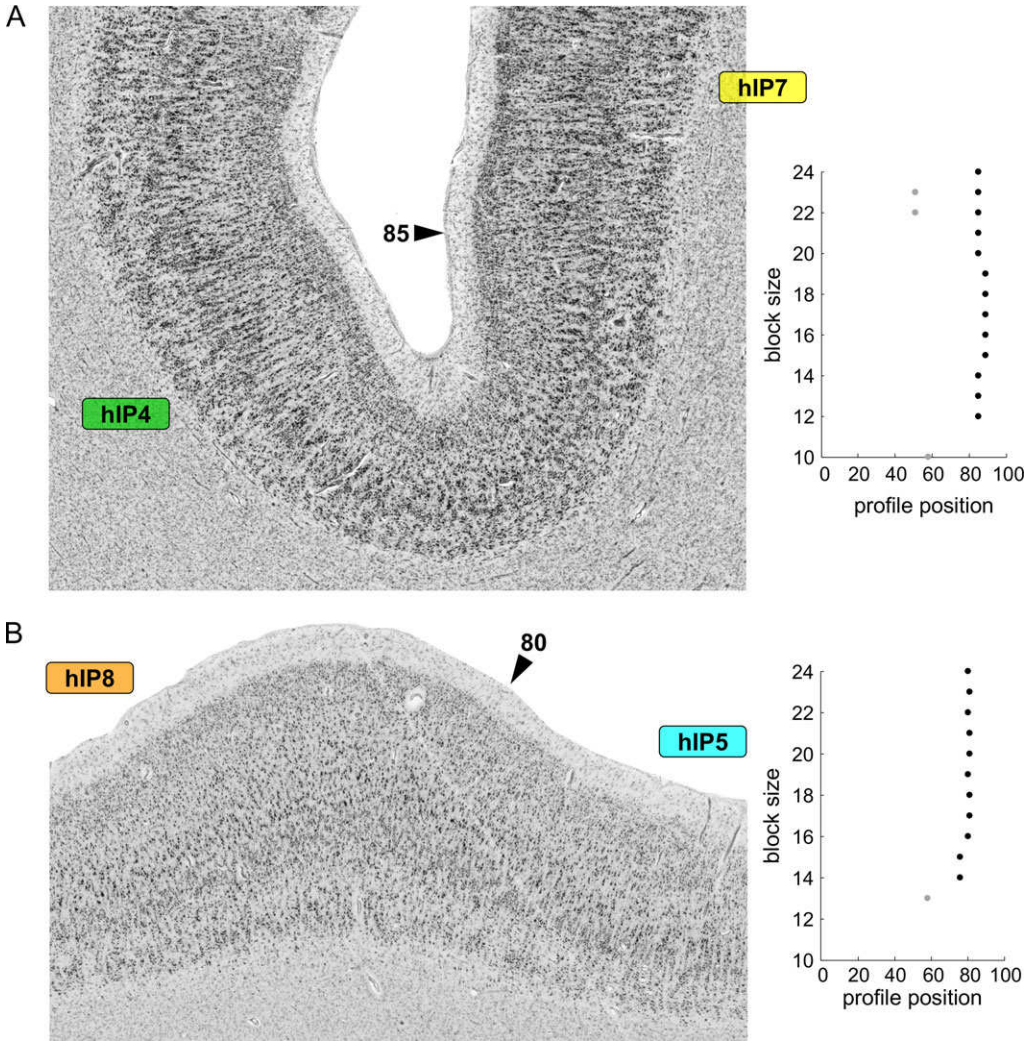


**Figure 7.** Cytoarchitectonic borders between (A) the lateral pIPS area hIP4 and medial pIPS area hIP7 at profile position 85 and between (B) medial pIPS area hIP8 and lateral pIPS area hIP5 at profile position 80 (marked with black arrows). On the right, the corresponding plots of significant ($P < 0.01$) maxima of the Mahalanobis distance function for different profile block sizes ($b = 10–24$) are depicted. Scale bars according to labeling within the figure.

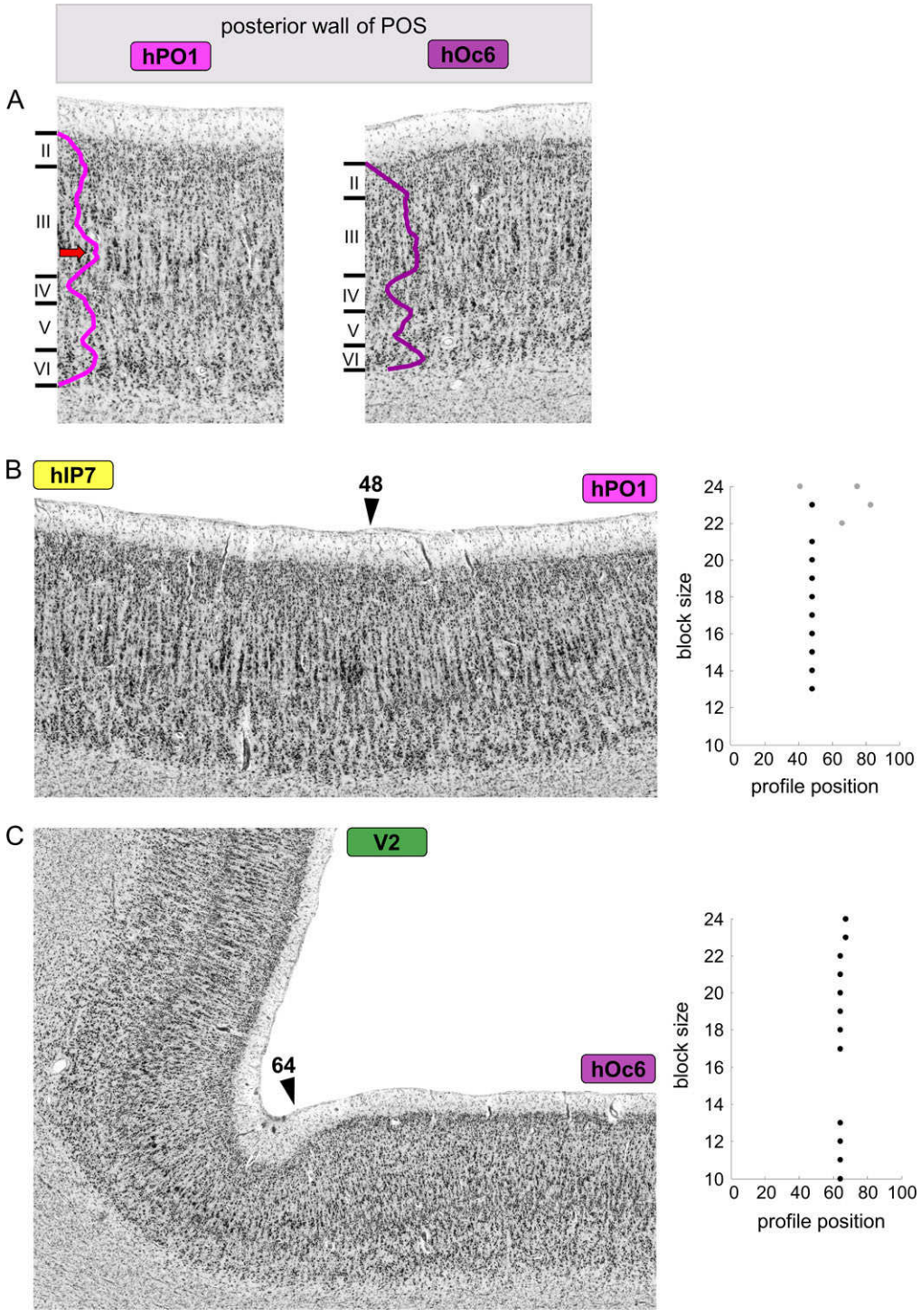


**Figure 8.** Cytoarchitecture of posterior wall of POS. (A) Cytoarchitectonic features of posterior wall of POS areas hPO1 and hOc6 within one investigated brain. Cytoarchitectonic borders between (B) hIP7 and hPO1 at profile position 48 and (C) hOc6 and V2 at profile position 64 (marked with black arrows). On the right, the corresponding plots of significant ($P < 0.01$) maxima of the Mahalanobis distance function for different profile block sizes ($b = 10–24$) are depicted. Scale bars according to labeling within the figure.

the cytoarchitectonic areas FG1, FG2 (Caspers et al. 2013), hOc4lp, hOc4la (Malikovic et al. 2016), hOc4d/V3A (Kujovic et al. 2013), and hOc5 (V5/MT+, Malikovic et al. 2007). Furthermore, subcortical coactivations were bilaterally found in the basal ganglia, including caudate nucleus, putamen, and pallidum, and the medial nuclear group of the thalamus.

Contrast analysis was performed by grouping hIP4, hIP7, hPO1 into a caudal cluster and hIP5,6,8 into a rostral cluster (grouping according to topographical location within the pIPS; Fig. 12B). The rostral cluster showed predominant functional connectivity with ventral and dorsal PMC, SMA and preSMA,

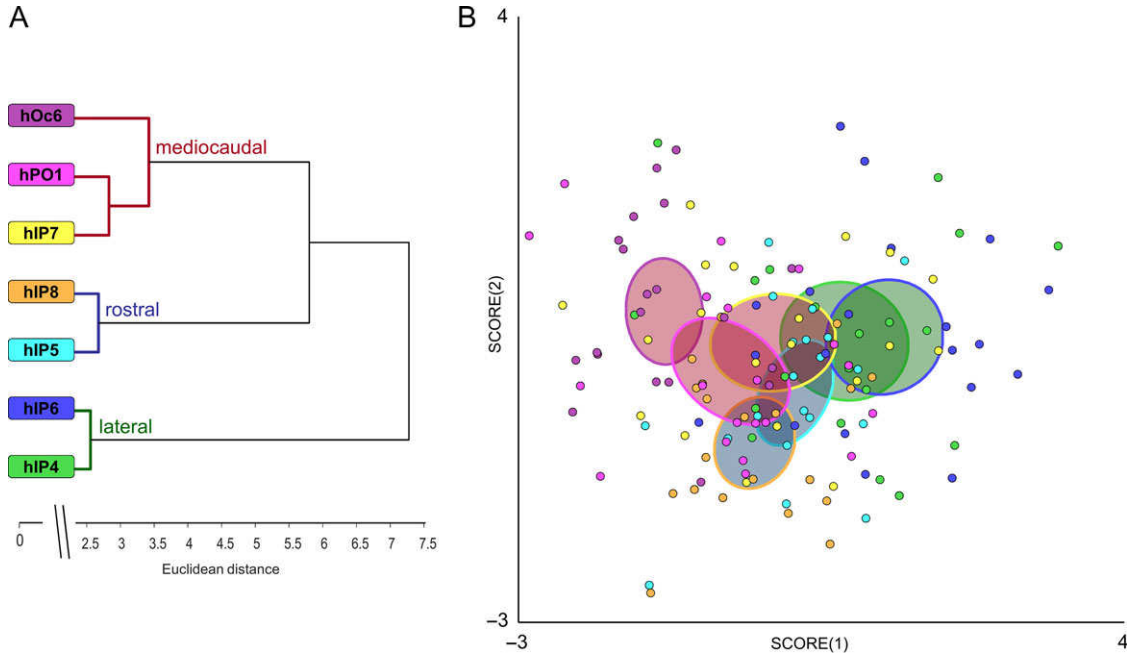


**Figure 9.** (A) Hierarchical cluster analysis (Ward linkage, Euclidean distances) and (B) analysis of multidimensional scaling (MDS) of the seven cytoarchitectonically distinct areas in pIPS and posterior wall of POS (averaged across left and right hemisphere). Three clusters were identified, whose areas showed similarities in cytoarchitecture: a mediocaudal (dark red), a rostral (dark blue) and a lateral (dark green) cluster; similar annotation within the MDS plot: respective filling colors of the ellipsoids (showing the confidence intervals) label membership of pIPS and adjacent posterior wall of POS area to respective cluster (from A). Outline colors of the ellipsoids denote the pIPS and adjacent posterior wall of POS area in accordance with the color code used throughout all figures.

vlPFC, anterior IPS areas hIP1, hIP2, hIP3, anterior insula and FO, the putamen and the medial nuclear group of the thalamus, as well as with the cerebellum. In contrast, the caudal cluster (hIP4,7, hPO1) showed more pronounced bilateral connectivity with ventral, dorsal and lateral occipital areas FG1, FG2, hOc4la, hOc4d/V3A and area hOc5 (V5/MT+). Taken together: the more rostral the areas were located, the higher the connectivity with motor and prefrontal regions.

## Discussion

The present study provides a complete cytoarchitectonic map of the human pIPS and adjacent posterior wall of POS. Using an image analysis and statistical tests, borders of seven distinct areas within the pIPS (hIP4-8) and adjacent posterior wall of POS (hPO1, hOc6) were found, and areas were mapped over their whole extent in series of histological sections of ten human postmortem brains. As a result, 3D-probability maps of the areas in pIPS and posterior POS in the MNI reference space were generated, enabling direct comparison with *in vivo* data from functional imaging studies. The probability maps were then used as seed regions to identify structure–function relationships and whole-brain connectivity patterns of each cytoarchitectonic area. Beside a common involvement of all these areas in spatial and visual perception, working memory and attention, a diagonal functional shift, i.e. change in functional assignment from visual information processing to higher cognitive functions, was identified when moving from caudo-medial to rostro-lateral areas of pIPS and posterior wall of POS. This diagonal shift of functional involvement goes hand in hand with a functional connectivity shift with (pre)frontal and temporo-occipital areas.

### Comparison of Present with Classical Maps of Human pIPS and Adjacent POS

In classical cytoarchitectonic human brain maps, e.g. by Brodmann (1909) or von Economo and Koskinas (1925), the IPS and adjacent POS were depicted as anatomical landmarks of the parietal and occipital lobes. In Brodmann's map, the IPS divides the PPC into SPL and IPL, separating inferior parietal areas BA40 and BA39 from superior parietal areas BA5 and BA7, whereas the adjacent POS separates parietal area BA7 from occipital area BA19 (Fig. 1). In the map of von Economo and Koskinas (1925), the IPS was also not parcellated in detail, but covered by two adjacent areas encroaching from the postcentral sulcus (area PD) and SPL (area PE) into the IPS. The adjacent POS was assigned to SPL area PEγ and occipital area OA. In contrast to these two maps, Gerhardt (1940) parcellated the region around and within the IPS into a mosaic of 15 areas, encompassing main areas 86–90 and corresponding subareas (Fig. 1). This parcellation was based on a single hemisphere, though, without replication of all findings in other brains, leaving this map largely neglected (Zilles and Palomero-Gallagher 2001). Thus, there is a mismatch between recent data on the organization of pIPS and posterior wall of POS as revealed by functional imaging studies in humans or cytoarchitectonical mapping studies in monkeys on the one hand, and current knowledge on the microstructural organization of this region in humans on the other. The current findings of five cytoarchitectonically distinct pIPS areas (hIP4-8) addressed this problem, providing a structural correlate for the functional heterogeneity of this region. The present maps extend previous research on anterior IPS (lateral wall: areas hIP1 and hIP2, Choi et al. 2006; medial wall: area hIP3, Scheperjans, Eickhoff et al. 2008; Scheperjans, Hermann et al. 2008).

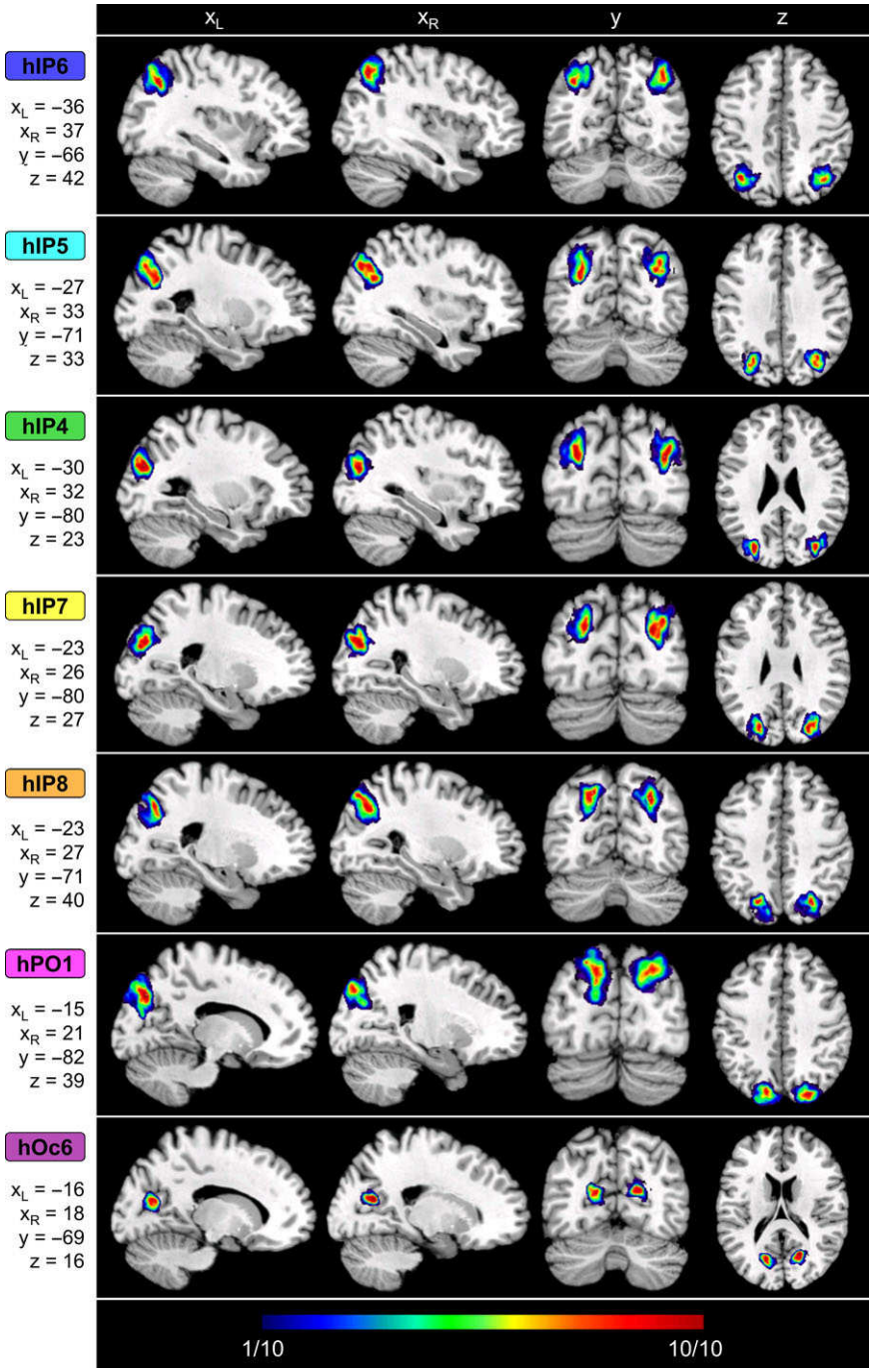


**Figure 10.** Continuous probability maps and stereotaxic coordinates of all areas in pIPS and posterior wall of POS in representative sagittal (left), coronal (middle), and horizontal (right) sections. 3D-probability maps show low probabilities (low overlap) in blue up to high probabilities (high-overlap) in red. Stereotaxic coordinates of the sections are given in the original Colin27-MNI reference space.

The newly described areas in pIPS areas were localized within the IPS, and rarely reach the lateral surface. This is in correspondence to the anterior IPS areas and the situation in monkeys (for an overview, see Grefkes and Fink 2005). In addition, two new areas within the adjacent posterior wall of POS (hPO1, hOc6) linked parietal with occipital cortex by common borders with visual areas like hOc4d/V3A, hOc3d/V3d, and hOc2/V2 (Amunts et al. 2000; Kujovic et al. 2013). The topographical attributes of the areas as belonging either to the parietal or occipital lobe were also reflected by their overall cytoarchitecture: the pIPS areas (hIP4-8) showed features of the "parietal type" as indicated by von Economo and Koskinas (1925), and were characterized by medium cortical width and medium-sized pyramidal cells in a broad layer III. Area hOc6 can be interpreted as the "polar type" with a smaller cortical width and a broader Layer IV. Lying at the transition between pIPS and POS, area hPO1 represents some kind of transitional area, showing aspects of both the parietal and polar type.

Extent and size of the areas varied between brains. The new maps of areas in pIPS and posterior wall POS accounted for this

**Table 2** Coordinates of the centers of gravity of continuous probability maps of each area in pIPS and posterior wall of POS within the original Colin27-MNI reference space (MNI) and the anatomical MNI space (aMNI; Amunts et al. 2005), based on 10 human postmortem brains.

| Area | Reference space | Center of gravity of probability maps | | | | | |
|---|---|---|---|---|---|---|---|
| | | Left hemisphere | | | Right hemisphere | | |
| | | x | y | z | x | y | z |
| hIP4 | MNI | −37 | −75 | 20 | 43 | −68 | 17 |
| | aMNI | −37 | −79 | 25 | 43 | −72 | 22 |
| hIP5 | MNI | −31 | −75 | 32 | 42 | −60 | 21 |
| | aMNI | −31 | −79 | 37 | 42 | −64 | 26 |
| hIP6 | MNI | −38 | −66 | 36 | 35 | −61 | 34 |
| | aMNI | −38 | −70 | 41 | 35 | −65 | 39 |
| hIP7 | MNI | −31 | −78 | 22 | 37 | −73 | 32 |
| | aMNI | −31 | −82 | 27 | 37 | −77 | 37 |
| hIP8 | MNI | −19 | −75 | 31 | 29 | −68 | 36 |
| | aMNI | −19 | −79 | 36 | 29 | −72 | 41 |
| hOc6 | MNI | −14 | −67 | 4 | 15 | −63 | 11 |
| | aMNI | −14 | −71 | 9 | 15 | −67 | 16 |
| hPO1 | MNI | −17 | −85 | 23 | 23 | −75 | 25 |
| | aMNI | −17 | −89 | 28 | 23 | −79 | 30 |

**Table 3** Corrected mean volumes [$mm^3$] and corresponding standard deviation (SD) of each area in pIPS and posterior wall of POS for the left and right hemisphere.

| Area | Corrected mean volume [$mm^3$] ± SD | |
|---|---|---|
| | Left hemisphere | Right hemisphere |
| hIP4 | 809.4 ± 172.1 | 782.9 ± 210.1 |
| hIP5 | 1009.9 ± 248.2 | 899.9 ± 328.6 |
| hIP6 | 1055.7 ± 162.5 | 897.4 ± 168.3 |
| hIP7 | 822.1 ± 238.3 | 909.5 ± 241.6 |
| hIP8 | 798.0 ± 154.3 | 874.8 ± 168.5 |
| hOc6 | 226.0 ± 42.4 | 237.3 ± 24.0 |
| hPO1 | 1404.0 ± 591.2 | 1304.4 ± 234.7 |

Histological volumes were corrected by the individual shrinkage factor F.

interindividual variability by integrating delineations from 10 individual brains. The final probability maps in the standard reference brain thus quantify for each voxel the likelihood of finding the given pIPS and POS area in this particular location. In contrast to classical brain maps, this allows quantitative assessment of structure–function relationships in this complex brain region. Part of this variability can be attributed to overall sulcal morphology, which particularly holds for the human IPS (present findings; Ono et al. 1990; Ebeling and Steinmetz 1995; Choi et al. 2006; Zlatkina and Petrides 2014), whereas human POS macroanatomically typically appears as a continuous sulcus (Ono et al. 1990; Malikovic et al. 2012). By non-linear registration of the individual delineations to the standard reference brain, these individual peculiarities in sulcal morphology are accounted for, with a good mapping of the diversity of the individual sulcal configurations on the anatomy of the pIPS and POS in the standard reference brain. Despite this variability, each area in pIPS and posterior wall of POS occupied a consistent core region (Fig 10, red) across individuals as depicted by the central high-overlap regions in the 3D-probability maps. Interindividual variability was lowest for area hOc6, though, which might be attributable to its constant position next to visual area V2, of which the location was also rather invariant (Amunts et al. 2000). The 3D-probability maps of pIPS and posterior wall of POS in the MNI reference space are directly comparable to results from neuroimaging studies to further analyze their functional role.

## Cytoarchitectonic Areas in Relation to Visuotopic Maps and Overall Brain Network Integration

As revealed by the present meta-analysis and known from numerous functional imaging studies, the IPS in general is involved in a large variety of tasks and functional domains. With the meta-analysis providing an overall organization of structure–function relationships in this brain region and as dedicated future studies are needed to reveal specific associations between the structural parcellation and the functional heterogeneity, the subsequent paragraphs focus on those aspects with contributed most to the observed functional shift across the IPS and adjacent POS areas.

Relating the new maps to visuotopically defined ones provides additional insight into their putative functional role. Visuotopic maps have been described repeatedly (Silver et al. 2005; Kastner et al. 2007; Swisher et al. 2007; Konen and Kastner 2008a; Silver and Kastner 2009; Henriksson et al. 2012) and recently published as a probabilistic atlas (Wang et al. 2015). Areas of this atlas along the caudo-rostral axis of the IPS, namely IPS0-IPS5 and SPL1, were identified using a memory-guided saccade task and covered mainly the medial bank of the IPS as well as adjacent aspects of superior parietal cortex. Overlaying these topographic maps with the 3D-probability maps of the new cytoarchitectonic areas identified in the present study reveals correspondences between area hIP7 of the present study and area IPS0 as well as between area hIP8 of the present study and area IPS1. Area hIP4 partially also overlapped with IPS0 within the bottom of pIPS. The other areas of the present study were located either medially (hPO1, hOc6) or laterally (hIP4, hIP5, hIP6) to these visuotopically defined areas by Wang et al. (2015). As the latter were identified using a visual task on memory-guided saccades, such correspondence between the here identified cytoarchitectonic areas hIP7 and hIP8 and the visuotopic maps IPS0 and IPS1 might provide first insight into the functional involvement of the newly described areas of the present study. The results of the present meta-analysis on general functional involvement and network integration of these areas across a multitude of individual neuroimaging studies provided additional insights into this putative structure–function correspondence. Similar to the memory-guided saccade task used to identify the visuotopic areas in PPC (Konen and Kastner 2008a; Silver and Kastner 2009; Wang et al. 2015), we also found consistent activation related to saccades in our meta-analysis particularly within these medial pIPS areas hIP7 and hIP8 which overlapped with the visuotopic areas IPS0 and IPS1. While these saccade-related activation patterns also spread to the medially adjacent area hPO1 in the posterior wall of POS, additional visual perceptive functions such as visual pursuit and tracking additionally involved laterally adjacent pIPS area hIP4. Such differential, but partially overlapping involvement of pIPS regions for these visual perceptive abilities might add to reports on different, but not completely separated processing streams (Berman et al. 1999; Petit and Haxby 1999; Silver and Kastner 2009). Linking this to cytoarchitectonic features showed that particularly these areas hPO1 and hIP7 shared

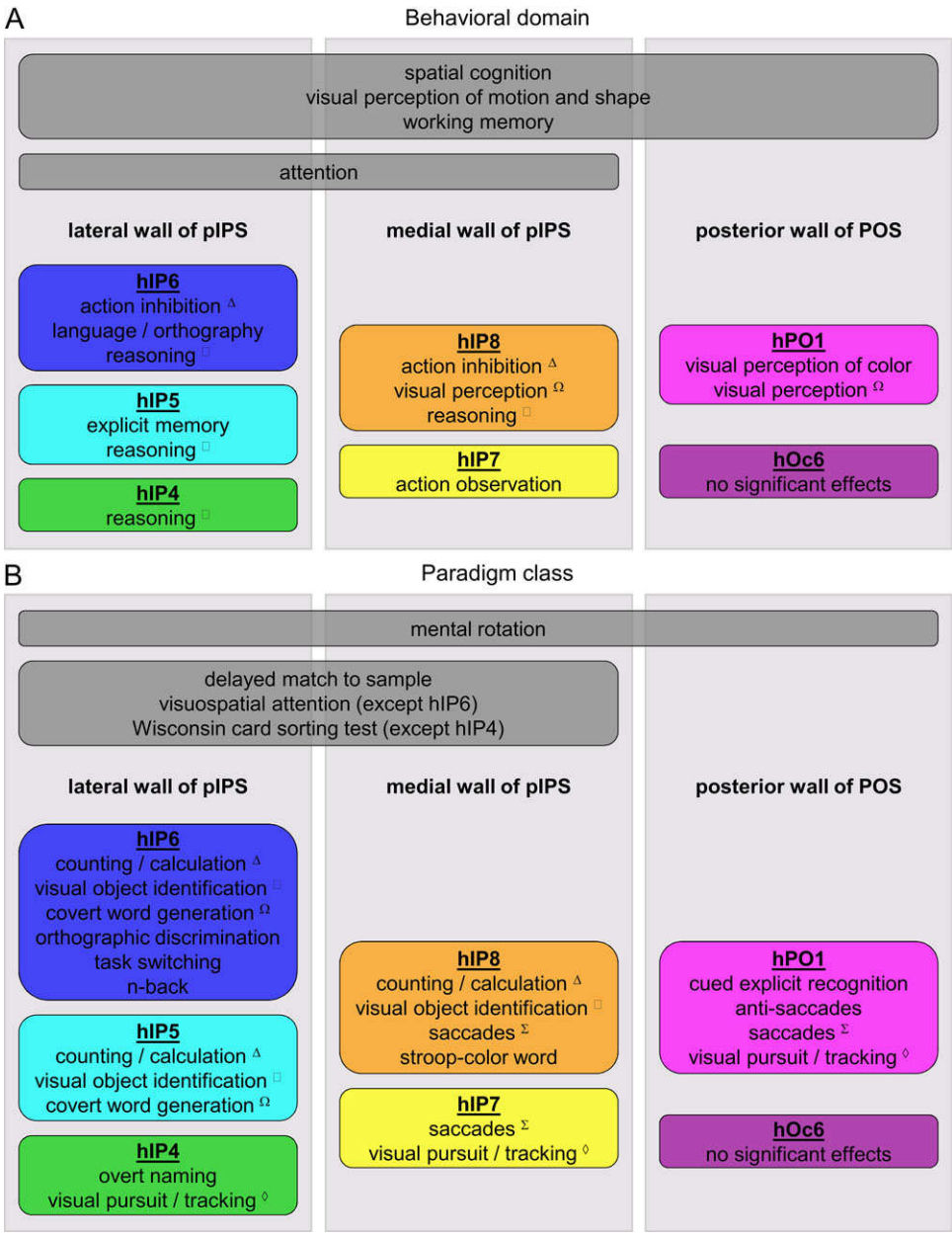


**Figure 11.** Meta-analytically derived insights into the overall organizational principles of functional involvement of the cytoarchitectonically defined areas in pIPS and posterior wall of POS. (A) Behavioral domains and (B) paradigm classes significantly associated with each pIPS and posterior wall of POS area, extracted from the BrainMap database. All areas in pIPS and posterior wall of POS were involved in spatial cognition, visual perception of motion and shape, working memory and activated during mental rotation tasks. All pIPS areas were involved in attention and activated during delayed match to sample tasks. Considering the methodical limitations of the performed quantitative meta-analysis, particular behavioral domains and paradigm classes, associated with only particular pIPS and posterior wall of POS areas, as well as common behavioral domains and paradigm classes (marked with a symbol), highlighted a diagonal functional shift within the pIPS and posterior wall of POS from rostral and lateral pIPS areas (hIP5,6) to mediocaudal pIPS and posterior wall of POS areas (hIP7, hPO1). Areas hIP4 and hIP8 represented transitional zones between these two poles.

common characteristics as revealed by the cytoarchitectonic cluster analysis, e.g., very prominent pyramidal cells in layer IIIc and high cell density in layer V, typical features of extrastriate visual areas (von Economo and Koskinas 1925; Amunts et al. 2000; Kujovic et al. 2013; Malikovic et al. 2007, 2016), underpinning their involvement in visual processing.

A further distinction between the pIPS and medially adjacent POS area hPO1 could also be revealed, though: While all pIPS and POS areas were involved in spatial cognition and working memory tasks, mainly in concert with several prefrontal regions (comparable to the so-called "task-positive network": Fox et al. 2005; Rottschy et al. 2012; Müller et al. 2015), only the pIPS areas were involved in attentional processes. The topographic maps IPS0 and IPS1 (Wang et al. 2015) identified using the memory-guided saccade task which particularly involved covert shifts of attention (Kastner et al. 2007; Konen and Kastner 2008a) overlapped with pIPS, but not POS areas. This might further hint at a distinction between basic extrastriate visual processing in hPO1 and higher associative visual and non-visual functions in pIPS.

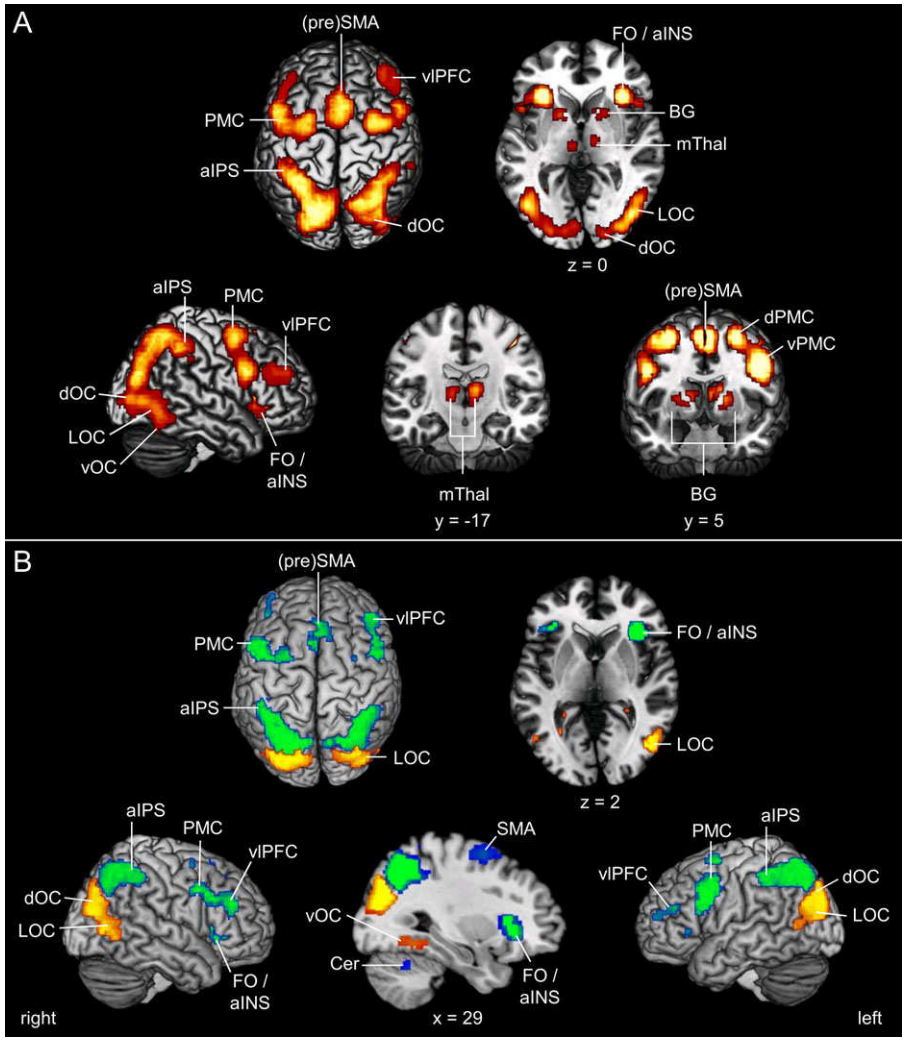


**Figure 12.** Significant results of MACM analysis. (A) Conjunction analysis of the coactivation maps of all areas in pIPS and posterior wall of POS, except hOc6, represented on the MNI-Colin27 reference brain. This bilateral network of significant coactivations included the ventral (vPMC) and dorsal premotor cortex (dPMC), (pre) supplementary motor area ((pre)SMA), ventrolateral prefrontal cortex (vlPFC), frontal operculum (FO) and anterior insula (aIns), area 44 (Broca region; Amunts et al. 1999), anterior IPS (aIPS) areas hIP1, hIP2 (Choi et al. 2006), and hIP3 (Scheperjans, Eickhoff et al. 2008; Scheperjans, Hermann et al. 2008), lateral occipital cortex (LOC): hOc4lp, hOc4la (Malikovic et al. 2016), and area hOc5 (V5/MT+, Malikovic et al. 2007), ventral occipital cortex (vOC): FG1, FG2 (Caspers et al. 2013), dorsal occipital cortex (dOC): hOc4d/V3A (Kujovic et al. 2013), as well as subcortical coactivations within the basal ganglia (BG), including caudate nucleus, putamen, and pallidum, and the medial nuclear group of the thalamus (mThal). (B) Contrast analysis between the coactivation maps of the caudal cluster (hIP4, hIP7, hPO1; yellow–orange) and the rostral cluster (hIP5,6,8; green–blue) on the MNI-Colin27 reference brain. The rostral cluster (green–blue) showed predominant functional connectivity with ventral and dorsal PMC, (pre)SMA, vlPFC, aIPS areas hIP1, hIP2, and hIP3, aIns and FO, the putamen and the medial nuclear group of the thalamus, as well as with the cerebellum (Cer). In contrast, the caudal cluster (yellow–orange) showed more pronounced bilateral connectivity with areas FG1, FG2, hOc4la, hOc4d/V3A and hOc5 (V5/MT+).

Furthermore, these focused relations between some of the visuotopic and some of the cytoarchitectonic maps of the present study suggest an overall differential involvement of the caudo-medio cytoarchitectonic areas of pIPS and POS in functional brain networks as compared with the laterally and rostrally adjacent cytoarchitectonic pIPS areas. For the visuotopic areas, higher functional and structural connectivity to early visual and adjacent temporal cortex for a posterior group of areas was described, while the anterior visuotopic IPS areas had stronger functional and structural connectivity with prefrontal areas (Uddin et al. 2010; Greenberg et al. 2012; Bray et al. 2013). The current contrast analysis of coactivation patterns complements these observations in terms of similar differences in functional connectivity: while caudal areas hIP4, hIP7, and hPO1 had stronger bilateral connectivity with early visual and occipito-temporal cortex, rostral areas hIP5, hIP6, and hIP8 were stronger connected with motor, frontal opercular and prefrontal cortex. This diagonal shift in connectivity from caudo-medial to rostro-lateral was indeed also reflected on the level of functional involvement in our present meta-analysis, with the rostro-lateral areas being more involved in higher cognitive functions such as reasoning, counting and calculation, or action inhibition.

The current database-driven meta-analytic approach was thus able to reveal a functional and connectional shift across the pIPS and POS areas identified in the present study, which is mirrored by a respective shift in cytoarchitectonic features of the areas. While the mediocaudal cluster of areas hIP7, hPO1, and hOc6 was characterized by large pyramidal cells in layer IIIc and thus resembled typical visual areas (see above), the

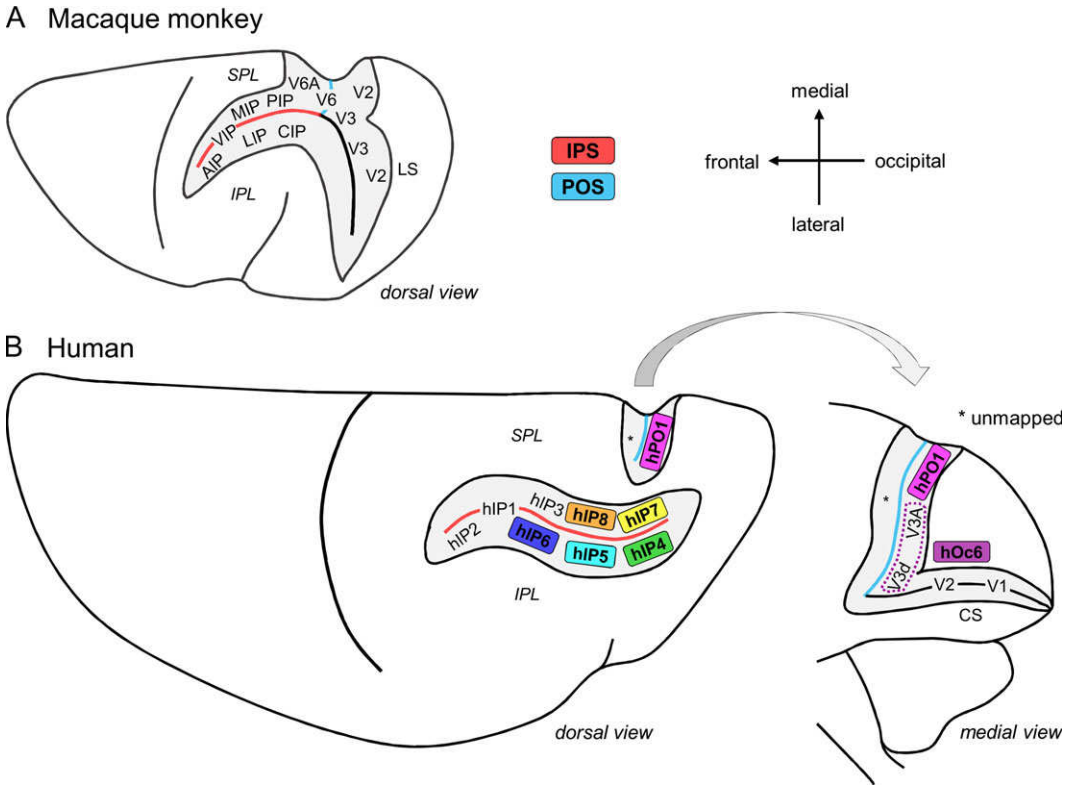


**Figure 13.** Comparison of IPS and adjacent POS parcellations in (A) the macaque monkey and (B) the human brain. The human parcellation is based on the newly defined areas of the present study (colored areas) as well as previously mapped areas in rostral IPS (hIP1, hIP2, hIP3: Choi et al. 2006; Scheperjans, Eickhoff et al. 2008; Scheperjans, Hermann et al. 2008) and primary, secondary and dorsal visual cortex (V1, V2: Amunts et al. 2000; V3A, V3d: Kujovic et al. 2013). The macaque monkey parcellation scheme is a summarized depiction of areas in IPS, POS and lunate sulcus (LS) in the left hemisphere (dorsal view, modified from Galletti et al. 2003). Relevant sulci are depicted open (in gray). Several distinct visual (V) and intraparietal (IP) areas, named after their topographical positions within the sulci, are labeled according to Felleman and van Essen 1991; Lewis and van Essen 2000; Cavada et al. 2000; Galletti et al. 2003; PIP = posterior IP, CIP = caudal IP, MIP = medial IP, LIP = lateral IP, VIP = ventral IP, AIP = anterior IP.

lateral and rostral areas all showed more homogeneously distributed medium-sized pyramidal cells typically associated with the parietal cortex type, particularly the inferior parietal cortex, with which rostro-lateral areas hIP4, hIP5, and hIP6 share common borders (von Economo and Koskinas 1925; Caspers et al. 2006, 2008). While these global shifts in microstructure and overall brain network integration might provide first hints, specific structure–function relationships of these newly identified cytoarchitectonic areas in human pIPS and adjacent posterior wall of POS need to be further elucidated in dedicated, well-controlled neuroimaging experiments. At this, methodical peculiarities of the performed meta-analysis need to be taken into account, such as effects of smoothing, generalization across a variety of studies under a summarizing label, relative selectivity of studies, behavioral domains and paradigm classes stored within the database and biased towards tasks in a standard scanner-setting (for additional information about potential and limitations of meta-analytic approaches, see e.g. Fox et al. 2014; Genon et al. 2018). The results of the current quantitative meta-analysis thus revealed a general organizational principle of structure–function relationships in human pIPS and adjacent POS and can thus serve as starting point for future dedicated assessments of the relation between functions and microstructurally defined areas using specific functional paradigms. This might have left relevant and well-studied abilities associated with pIPS, such as the ability to process 3D visual information which might involve caudal IPS and adjacent dorsal visual stream (Tsao et al. 2003; Jastorff et al. 2016; Welchmann 2016), or the question of specific vs. unspecific activations as, e.g. the case for action observation for which highly specific activations are typically found in rostral IPS (Ferri et al. 2015; Corbo and Orban 2017), out of the picture. It might also explain why for POS area hOc6 no significant associations with particular functions were found. Here, the cytoarchitectonic cluster analysis might provide additional insight that hOc6 might be involved in similar functions as areas hIP7 and hPO1 as they together form the mediocaudal cytoarchitectonic cluster.

## Similar Topographical Arrangement of Areas in Human and Monkey pIPS and POS

The new maps of human pIPS and adjacent posterior wall of POS could furthermore add to the discussion on putative homologies in this region between humans and monkeys (for review: Grefkes and Fink 2005).

Focusing only on topographical organizational principles within monkey and human IPS and POS, a prominent similarity in number and topographical arrangement of pIPS and POS areas in humans and monkeys can be observed (Fig. 13). In both species, cytoarchitectonically identified areas are located mainly on a particular wall of the IPS or POS, either on the lateral or the medial wall. Additionally, all identified areas reside within the sulcus and hardly extend onto the free surface (for

the monkey IPS see e.g., Grefkes and Fink 2005). In monkeys, the lateral wall of the IPS consists (from rostral to caudal) of areas AIP, VIP (in the bottom of the sulcus, potential subdivision into VIPm and VIPl), LIP (potential subdivision into LIPv and LIPd), and CIP (Seltzer and Pandya 1986, 1980; Colby et al. 1988; Andersen et al. 1990; Blatt et al. 1990; Felleman and van Essen 1991; Cavada et al. 2000; Lewis and van Essen 2000; Galletti et al. 2003). In a similar topographical arrangement from rostral to caudal, the lateral wall of human IPS consists of areas hIP2, hIP1 (in the bottom of the sulcus), hIP6, hIP5, and hIP4. Thus, in both species, there is a comparable topography with 4–5 rostro-caudally arranged distinct areas. The same holds true for the medial wall of IPS: in monkeys, there are from rostral to caudal medial area MIP and posterior area PIP, whereas in humans, there are (also from rostral to caudal) areas hIP3, hIP8, and hIP7. The overall topography of areas in human and monkey IPS seems to be comparable. Whether this topographical comparability relates to microstructural and functional similarity needs to be elucidated in future dedicated comparative studies. It could, e.g. be shown that typical lateral IPS functions (such as involvement in visuospatial attention and saccades) in monkeys is covered by medially located IPS areas and adjacent cortical regions in humans (for review, see Grefkes and Fink 2005; Orban 2016), which is further supported by our current meta-analysis (see section 4.2). The present results might add the yet missing link on putative structural–functional homologies in human and monkey IPS by providing maps of microstructurally defined, yet unavailable areas for human pIPS.

The topography of areas in the posterior wall of POS in monkeys and humans appears not as comparable as for the pIPS. In monkeys, the posterior wall of POS is mainly covered by dorsal parts of visual areas V2 and V3 (Gamberini et al. 2015), followed by area V6 in the bottom of the sulcus and area V6A (PO), which is already located on the anterior wall (Galletti et al. 1996, 1997, 2003; Gamberini et al. 2015). In humans, though, areas hOc2 (V2), hOc3d (V3d), and hOc4d (V3A) were mainly located within the occipital lobe, only encroaching on the posterior wall of POS (Amunts et al. 2000; Kujovic et al. 2013). Area hPO1 identified in the present study filled the yet uncharted part of the posterior wall of human POS, adjacent to area V3A and the also newly identified area hOc6 caudally and in close proximity to medial pIPS area hIP7 and hIP8 (Fig. 13), resembling the situation for area V6A in monkeys. The here described areas in the posterior wall of human POS (hPO1, hOc6) might provide an additional structural basis for further elucidating the potential homology in this region, including the discussion on potential human homologs of areas V6 and V6A (Tzelepi et al. 2001; Vanni et al. 2001; Dechent and Frahm 2003; Fattori et al. 2009; Cavina-Pratesi et al. 2010; Pitzalis et al. 2006, 2010, 2015).

## Conclusions

The present study provides the first cytoarchitectonical maps of human pIPS and adjacent posterior wall of POS using an observer-independent, quantitative mapping approach in 10 human post mortem brains. Seven cytoarchitectonically distinct areas within pIPS (hIP4-8) and adjacent posterior wall of POS (hPO1, hOc6) were identified. Beside the common functional involvement of all areas in pIPS and posterior wall of POS, except hOc6, in visuomotor integration, working memory and attention, a diagonal functional shift within human pIPS and adjacent POS from visual processing to higher cognitive functions like orthography and calculation could be established as a major organizational principle in this region, mirrored by differential functional connectivity with (pre)frontal and temporo-occipital areas. The architectonical complexity of human pIPS and adjacent POS and the resulting functional and connectional diversity may contribute to the understanding of the functional relevance of human IPS and adjacent POS for visual processing and cognitive functions. These new 3D cytoarchitectonic maps of human pIPS and adjacent POS can now be used as an anatomical fundament to link the functional heterogeneity of this region to a similarly complex mosaic of structural areas.

## Supplementary Material

Supplementary material is available at *Cerebral Cortex* online.

## Funding

Funding was granted by the Initiative and Networking Fund of the Helmholtz Association (S.C.), the portfolio theme "Supercomputing and Modeling for the Human Brain" by the Helmholtz Association (K.A., K.Z.) as well as and funding from the European Union's Horizon 2020 Research and Innovation Programme under Grant Agreement No. **720270** (HBP SGA1; K.A., K.Z., S.B.E.) and No. **785907** (HBP SGA2; K.A., K.Z., S.B.E., S.C.).

## Notes

*Conflict of Interest*: None declared.

## References

Amunts K, Kedo O, Kindler M, Pieperhoff P, Mohlberg H, Shah NJ, Habel U, Schneider F, Zilles K. 2005. Cytoarchitectonic mapping of the human amygdala, hippocampal region and entorhinal cortex: intersubject variability and probability maps. Anat Embryol (Berl). 210:343–352.

Amunts K, Malikovic A, Mohlberg H, Schormann T, Zilles K. 2000. Brodmann's areas 17 and 18 brought into stereotaxic space—where and how variable? Neuroimage. 11(1):66–84.

Amunts K, Schleicher A, Bürgel U, Mohlberg H, Uylings HBM, Zilles K. 1999. Broca's region revisited: cytoarchitecture and intersubject variability. J Comp Neurol. 412:319–341.

Amunts K, Schleicher A, Zilles K. 2007. Cytoarchitecture of the cerebral cortex—more than localization. Neuroimage. 37: 1061–1065.

Amunts K, Zilles K. 2015. Architectonic mapping of the human brain beyond Brodmann. Neuron. 88(6):1086–1107.

Andersen RA, Bracewall RM, Barash S, Gnadt JW, Fogassi L. 1990. Eye position effects on visual, memory, and saccade-related activity in areas LIP and 7a of Macaque. J Neurosci. 10(4):1176–1196.

Astafiev SV, Shulman GL, Stanley CM, Snyder AZ, van Essen DC, Corbetta M. 2003. Functional organization of human intraparietal and frontal cortex for attending, looking, and pointing. J Neurosci. 23:4689–4699.

Barton B, Brewer AA. 2013. Visual working memory in human cortex. Psychology (Irvine). 4(8):655–662.

Berman RA, Colby CL, Genovese CR, Voyvodic JT, Luna B, Thulborn KR, Sweeney JA. 1999. Cortical networks subserving pursuit and saccadic eye movements in humans: an FMRI study. Hum Brain Mapp. 8:209–225.

Bettencourt KC, Xu Y. 2016. Understanding location- and feature-based processing along the human intraparietal sulcus. J Neurophysiol. 116(3):1488–1497.

Binkofski FC, Klann J, Caspers S. 2015. On the neuroanatomy and functional role of the inferior parietal lobule and intraparietal sulcus. In: Hickok G, Small SL, editors. Neurobiology of Language. Amsterdam: Academic Press. p. 35–47.

Blatt GJ, Andersen RA, Stoner GR. 1990. Visual receptive field organization and cortico-cortical connections of the lateral intraparietal area (area LIP) in the macaque. J Comp Neurol. 299(4):421–445.

Bludau S, Eickhoff SB, Mohlberg H, Caspers S, Laird AR, Fox PT, Schleicher A, Zilles K, Amunts K. 2014. Cytoarchitecture, probability maps and functions of the human frontal pole. Neuroimage. 93:260–275.

Bray S, Almas R, Arnold AEGF, Iaria G, MacQueen G. 2015. Intraparietal sulcus activity and functional connectivity supporting spatial working memory manipulation. Cereb Cortex. 25(5):1252–1264.

Bray S, Arnold AEGF, Iaria G, MacQueen G. 2013. Structural connectivity of visuotopic intraparietal sulcus. Neuroimage. 82: 137–145.

Brodmann K. 1909. Vergleichende Lokalisationslehre der Großhirnrinde. Leipzig: Verlag von Johann Ambrosius Barth.

Caspers J, Zilles K, Eickhoff SB, Schleicher A, Mohlberg H, Amunts K. 2013. Cytoarchitectonical analysis and probabilistic mapping of two extrastriate areas of the human posterior fusiform gyrus. Brain Struct Funct. 218(2):511–526.

Caspers S, Eickhoff SB, Geyer S, Scheperjans F, Mohlberg H, Zilles K, Amunts K. 2008. The human inferior parietal lobule in stereotaxic space. Brain Struct Funct. 212(6):481–495.

Caspers S, Geyer S, Schleicher A, Mohlberg H, Amunts K, Zilles K. 2006. The human inferior parietal cortex: cytoarchitectonic parcellation and interindividual variability. Neuroimage. 33 (2):430–448.

Cavada C, Company T, Tejedor J, Cruz-Rizzolo RJ, Reinoso-Suárez F. 2000. The anatomical connections of the Macaque Monkey orbitofrontal cortex. A Review. Cereb Cortex. 10(3): 220–242.

Cavina-Pratesi C, Monaco S, Fattori P, Galletti C, McAdam TD, Quinlan DJ, Goodale MA, Culham JC. 2010. Functional magnetic resonance imaging reveals the neural substrates of arm transport and grip formation in reach-to-grasp actions in humans. J Neurosci. 30(31):10306–10323.

Choi H-J, Zilles K, Mohlberg H, Schleicher A, Fink GR, Armstrong E, Amunts K. 2006. Cytoarchitectonic identification and probabilistic mapping of two distinct areas within the anterior ventral bank of the human intraparietal sulcus. J Comp Neurol. 495(1):53–69.

Colby CL, Gattas R, Olson CR, Gross CG. 1988. Topographical organization of cortical afferents to extrastriate visual area PO in the macaque: a dual tracer study. J Comp Neurol. 269: 392–413.

Colby CL, Goldberg ME. 1999. Space and attention in parietal cortex. Annu Rev Neurosci. 22:319–349.

Corbetta M, Akbudak E, Conturo TE, Snyder AZ, Ollinger JM, Drury HA, Linenweber MR, Petersen SE, Raichle ME, van Essen DC, et al. 1998. A common network of functional areas for attention and eye movements. Neuron. 21(4):761–773.

Corbetta M, Shulman GL. 2002. Control of goal-directed and stimulus-driven attention in the brain. Nat Rev Neurosci. 3 (3):201–215.

Corbo D, Orban GA. 2017. Observing others speak or sing activates Spt and neighboring parietal regions. J Cogn Neurosci. 29:1002–1021.

Coull JT, Frith CD. 1998. Differential activation of right superior parietal cortex and intraparietal sulcus by spatial and nonspatial attention. Neuroimage. 8(2):176–187.

Culham JC, Brandt SA, Cavanagh P, Kanwisher NG, Dale AM, Tootell RBH. 1998. Cortical fMRI activation produced by attentive tracking of moving targets. J Neurophysiol. 80(5): 2657–2670.

Culham JC, Kanwisher NG. 2001. Neuroimaging of cognitive functions in human parietal cortex. Curr Opin Neurobiol. 11: 157–163.

Dechent P, Frahm J. 2003. Characterization of the human visual V6 complex by functional magnetic resonance imaging. Eur J Neurosci. 17(10):2201–2211.

Dehaene S. 2009. Origins of mathematical intuitions: the case of arithmetic. Ann NY Acad Sci. 1156:232–259.

Dehaene S, Dehaene-Lambertz G, Cohen L. 1998. Abstract representations of numbers in the animal and human brain. Trends Neurosci. 21(8):355–361.

Dehaene S, Piazza M, Pinel P, Cohen L. 2003. Three parietal circuits for number processing. Cogn Neuropsychol. 20(3): 487–506.

Denys K, Vanduffel W, Fize D, Nelissen K, Peuskens H, van Essen D, Orban GA. 2004. The processing of visual shape in the cerebral cortex of human and nonhuman primates: a functional magnetic resonance imaging study. J Neurosci. 24(10):2551–2565.

Durand J-B, Peeters R, Norman JF, Todd JT, Orban GA. 2009. Parietal regions processing visual 3D shape extracted from disparity. Neuroimage. 46(4):1114–1126.

Ebeling U, Steinmetz H. 1995. Anatomy of the parietal lobe: mapping the individual pattern. Acta Neurochir (Wien). 136: 8–11.

Eickhoff SB, Bzdok D, Laird AR, Kurth F, Fox PT. 2012. Activation likelihood estimation meta-analysis revisited. Neuroimage. 59(3):2349–2361.

Eickhoff SB, Bzdok D, Laird AR, Roski C, Caspers S, Zilles K, Fox PT. 2011. Co-activation patterns distinguish cortical modules, their connectivity and functional differentiation. Neuroimage. 57(3):938–949.

Eickhoff SB, Heim S, Zilles K, Amunts K. 2006. Testing anatomically specified hypotheses in functional imaging using cytoarchitectonic maps. Neuroimage. 32(2):570–582.

Eickhoff SB, Laird AR, Grefkes C, Wang LE, Zilles K, Fox PT. 2009. Coordinate-based activation likelihood estimation meta-analysis of neuroimaging data: a random-effects approach based on empirical estimates of spatial uncertainty. Hum Brain Mapp. 30(9):2907–2926.

Eickhoff SB, Nichols TE, Laird AR, Hoffstaedter F, Amunts K, Fox PT, Bzdok D, Eickhoff CR. 2016. Behavior, sensitivity, and power of activation likelihood estimation characterized by massive empirical simulation. Neuroimage. 137: 70–85.

Eickhoff SB, Stephan KE, Mohlberg H, Grefkes C, Fink GR, Amunts K, Zilles K. 2005. A new SPM toolbox for combining probabilistic cytoarchitectonic maps and functional imaging data. Neuroimage. 25(4):1325–1335.

Evans AC, Marrett S, Neelin P, Collins L, Worsley K, Dai W, Milot S, Meyer E, Bub D. 1992. Anatomical mapping of functional activation in stereotactic coordinate space. Neuroimage. 1(1):43–53.

Fattori P, Pitzalis S, Galletti C. 2009. The cortical visual area V6 in macaque and human brains. J Physiol Paris. 103:88–97.

Felleman DJ, van Essen DC. 1991. Distributed hierarchical processing in the primate cerebral cortex. Cereb Cortex. 1:1–47.

Ferri S, Rizzolatti G, Orban GA. 2015. The organization of the posterior parietal cortex devoted to upper limb actions: an fMRI study. Hum Brain Mapp. 36:3845–3866.

Fox MD, Snyder AZ, Vincent JL, Corbetta M, van Essen DC, Raichle ME. 2005. The human brain is intrinsically organized into dynamic, anticorrelated functional networks. Proc Natl Acad Sci USA. 102(27):9673–9678.

Fox PT, Lancaster JL. 2002. Mapping context and content: the BrainMap model. Nat Rev Neurosci. 3(4):319–321.

Fox PT, Lancaster JL, Laird AR, Eickhoff SB. 2014. Meta-analysis in human neuroimaging: computational modeling of large-scale databases. Annu Rev Neurosci. 37:409–434.

Galletti C, Fattori P, Battaglini PP, Shipp S, Zeki S. 1996. Functional demarcation of a border between areas V6 and V6A in the superior parietal gyrus of the Macaque monkey. Eur J Neurosci. 8(1):30–52.

Galletti C, Fattori P, Kutz DF, Battaglini PP. 1997. Arm movement-related neurons in the visual area V6A of the Macaque superior parietal lobule. Eur J Neurosci. 9:410–413.

Galletti C, Kutz DF, Gamberini M, Breveglieri R, Fattori P. 2003. Role of the medial parieto-occipital cortex in the control of reaching and grasping movements. Exp Brain Res. 153(2): 158–170.

Gamberini M, Fattori P, Galletti C. 2015. The medial parietal occipital areas in the macaque monkey. Vis Neurosci. 32: 1–13.

Genon S, Reid A, Langner R, Amunts K, Eickhoff SB. 2018. How to characterize the function of a brain region. Trends Cogn Sci. 22(4):350–364.

Gerhardt E. 1940. Die Cytoarchitektonik des Isocortex parietalis beim Menschen. J Psychol Neurol. 49:367–419.

Geyer S, Schormann T, Mohlberg H, Zilles K. 2000. Areas 3a, 3b, and 1 of human primary somatosensory cortex. Part 2. Spatial normalization to standard anatomical space. NeuroImage. 11(6 Pt 1):684–696.

Geyer S, Schleicher A, Zilles K. 1999. Areas 3a, 3b, and 1 of human primary somatosensory cortex. NeuroImage. 10(1): 63–83.

Greenberg AS, Verstynen T, Chiu Y-C, Yantis S, Schneider W, Behrmann M. 2012. Visuotopic cortical connectivity underlying attention revealed with white-matter tractography. J Neurosci. 32(8):2773–2782.

Grefkes C, Geyer S, Schormann T, Roland P, Zilles K. 2001. Human somatosensory area 2. NeuroImage. 14(3):617–631.

Grefkes C, Fink GR. 2005. REVIEW: the functional organization of the intraparietal sulcus in humans and monkeys. J Anat. 207:3–17.

Henriksson L, Karvonen J, Salminen-Vaparanta N, Railo H, Vanni S. 2012. Retinotopic maps, spatial tuning, and locations of human visual areas in surface coordinates characterized with multifocal and blocked FMRI designs. PLoS One. 7(5):e36859.

Hömke L. 2006. A multigrid method for anisotropic PDEs in elastic image registration. Numer Linear Algebra Appl. 13: 215–229.

Husain M, Nachev P. 2007. Space and the parietal cortex. Trends Cogn Sci. 11(1):30–36.

Jastorff J, Abdollahi RO, Fasano F, Orban GA. 2016. Seeing biological actions in 3D: an fMRI study. Hum Brain Mapp. 37(1): 203–219.

Kastner S, DeSimone K, Konen CS, Szczepanski SM, Weiner KS, Schneider KA. 2007. Topographic maps in human frontal cortex revealed in memory-guided saccade and spatial working-memory tasks. J Neurophysiol. 97(5):3494–3507.

Kertzman C, Schwarz U, Zeffiro TA, Hallett M. 1997. The role of posterior parietal cortex in visually guided reaching movements in humans. Exp Brain Res. 114(1):170–183.

Konen CS, Kastner S. 2008a. Representation of eye movements and stimulus motion in topographically organized areas of human posterior parietal cortex. J Neurosci. 28(33): 8361–8375.

Konen CS, Kastner S. 2008b. Two hierarchically organized neural systems for object information in human visual cortex. Nat Neurosci. 11(2):224–231.

Konen CS, Mruczek REB, Montoya JL, Kastner S. 2013. Functional organization of human posterior parietal cortex: grasping- and reaching-related activations relative to topographically organized cortex. J Neurophysiol. 109(12): 2897–2908.

Kujovic M, Zilles K, Malikovic A, Schleicher A, Mohlberg H, Rottschy C, Eickhoff SB, Amunts K. 2013. Cytoarchitectonic mapping of the human dorsal extrastriate cortex. Brain Struct Funct. 218(1):157–172.

LaBar KS, Gitelman DR, Parrish TB, Mesulam M. 1999. Neuroanatomic overlap of working memory and spatial attention networks: a functional MRI comparison within subjects. Neuroimage. 10(6):695–704.

Lacadie CM, Fulbright RK, Rajeevan N, Constable RT, Papademetris X. 2008. More accurate Talairach coordinates for neuroimaging using non-linear registration. Neuroimage. 42(2):717–725.

Laird AR, Eickhoff SB, Kurth F, Fox PM, Uecker AM, Turner JA, Robinson JL, Lancaster JL, Fox PT. 2009. ALE meta-analysis workflows via the BrainMap database: progress towards a probabilistic functional brain Atlas. Front Neuroinform. 3: 1–23.

Laird AR, Lancaster JL, Fox PT. 2005. BrainMap: the social evolution of a human brain mapping database. Neuroinformatics. 3:65–77.

Lewis JW, van Essen DC. 2000. Mapping of architectonic subdivisions in the macaque monkey, with emphasis on parieto-occipital cortex. J Comp Neurol. 428(1):79–111.

Lorenz S, Weiner KS, Caspers J, Mohlberg H, Schleicher A, Bludau S, Eickhoff SB, Grill-Spector K, Zilles K, Amunts K. 2017. Two new cytoarchitectonic areas on the human mid-fusiform gyrus. Cereb Cortex. 27:373–385.

Mahalanobis PC, Majumdar DN, Rao CR. 1949. Anthropometric survey of the United Provinces, 1941: a statistical study. Sankya. 9:89–324.

Malikovic A, Amunts K, Schleicher A, Mohlberg H, Eickhoff SB, Wilms M, Palomero-Gallagher N, Armstrong E, Zilles K. 2007. Cytoarchitectonic analysis of the human extrastriate cortex in the region of V5/MT+: a probabilistic, stereotaxic map of area hOc5. Cereb Cortex. 17(3):562–574.

Malikovic A, Amunts K, Schleicher A, Mohlberg H, Kujovic M, Palomero-Gallagher N, Eickhoff SB, Zilles K. 2016. Cytoarchitecture of the human lateral occipital cortex: mapping of two extrastriate areas hOc4la and hOc4lp. Brain Struct Funct. 221(4):1877–1897.

Malikovic A, Vucetic B, Milisavljevic M, Tosevski J, Sazdanovic P, Milojevic B, Malobabic S. 2012. Occipital sulci of the human brain: variability and morphometry. Anat Sci Int. 87 (2):61–70.

Mars RB, Jbabdi S, Sallet J, O'Reilly JX, Croxson PL, Olivier E, Noonan MP, Bergmann C, Mitchell AS, Baxter MG, et al. 2011. Diffusion-weighted imaging tractography-based

parcellation of the human parietal cortex and comparison with human and macaque resting-state functional connectivity. J Neurosci. 31(11):4087–4100.
Merker B. 1983. Silver staining of cell bodies by means of physical development. J Neurosci Methods. 9(3):235–241.
Müller VI, Langner R, Cieslik EC, Rottschy C, Eickhoff SB. 2015. Interindividual differences in cognitive flexibility: influence of gray matter volume, functional connectivity and trait impulsivity. Brain Struct Funct. 220(4):2401–2414.
Nichols T, Brett M, Andersson J, Wager T, Poline J-B. 2005. Valid conjunction inference with the minimum statistic. Neuroimage. 25(3):653–660.
Nieder A. 2005. Counting on neurons: the neurobiology of numerical competence. Nat Rev Neurosci. 6(3):177–190.
Offen S, Gardner JL, Schluppeck D, Heeger DJ. 2010. Differential roles for frontal eye fields (FEFs) and intraparietal sulcus (IPS) in visual working memory and visual attention. J Vis. 10(11):28.
Ono M, Kubik S, Abernathey CD. 1990. Atlas of the Cerebral Sulci. Stuttgart: Thieme.
Orban GA. 2016. Functional definitions of parietal areas in human and non-human primates. Proc Biol Sci. 283(1828): 1–9.
Orban GA, Claeys K, Nelissen K, Smans R, Sunaert S, Todd JT, Wardak C, Durand J-B, Vanduffel W. 2006. Mapping the parietal cortex of human and non-human primates. Neuropsychologia. 44(13):2647–2667.
Orban GA, van Essen D, Vanduffel W. 2004. Comparative mapping of higher visual areas in monkeys and humans. Trends Cogn Sci. 8(7):315–324.
Pessoa L, Gutierrez E, Bandettini PA, Ungerleider LG. 2002. Neural correlates of visual working memory: fMRI amplitude predicts task performance. Neuron. 35:975–987.
Petit L, Haxby JV. 1999. Functional anatomy of pursuit eye movements in humans as revealed by fMRI. J Neurophysiol. 81:463–471.
Pitzalis S, Fattori P, Galletti C. 2015. The human cortical areas V6 and V6A. Vis Neurosci. 32:E007.
Pitzalis S, Galletti C, Huang R-S, Patria F, Committeri G, Galati G, Fattori P, Sereno MI. 2006. Wide-field retinotopy defines human cortical visual area v6. J Neurosci. 26(30):7962–7973.
Pitzalis S, Sereno MI, Committeri G, Fattori P, Galati G, Patria F, Galletti C. 2010. Human v6: the medial motion area. Cereb Cortex. 20(2):411–424.
Raabe M, Fischer V, Bernhardt D, Greenlee MW. 2013. Neural correlates of spatial working memory load in a delayed match-to-sample saccade task. Neuroimage. 71:84–91.
Riedel MC, Ray K, Fox PM, Uecker AM, Eickhoff SB, Fox PT, Laird AMR. 2013. BrainMap. In: Jaeger D, Jung R, editors. Encyclopedia of Computational Neuroscience. New York: Springer. p. 1–3.
Robinson JL, Laird AR, Glahn DC, Lovallo WR, Fox PT. 2010. Metaanalytic connectivity modeling: delineating the functional connectivity of the human amygdala. Hum Brain Mapp. 31(2):173–184.
Rosen ML, Stern CE, Michalka SW, Devaney KJ, Somers DC. 2015. Influences of long-term memory-guided attention and stimulus-guided attention on visuospatial representations within human intraparietal sulcus. J Neurosci. 35(32): 11358–11363.
Rottschy C, Langner R, Dogan I, Reetz K, Laird AR, Schulz JB, Fox PT, Eickhoff SB. 2012. Modelling neural correlates of working memory: a coordinate-based meta-analysis. Neuroimage. 60 (1):830–846.
Sack AT. 2009. Parietal cortex and spatial cognition. Behav Brain Res. 202(2):153–161.
Scheperjans F, Eickhoff SB, Homke L, Mohlberg H, Hermann K, Amunts K, Zilles K. 2008. Probabilistic maps, morphometry, and variability of cytoarchitectonic areas in the human superior parietal cortex. Cereb Cortex. 18(9):2141–2157.
Scheperjans F, Hermann K, Eickhoff SB, Amunts K, Schleicher A, Zilles K. 2008. Observer-independent cytoarchitectonic mapping of the human superior parietal cortex. Cereb Cortex. 18(4):846–867.
Schleicher A, Amunts K, Geyer S, Morosan P, Zilles K. 1999. Observer-independent method for microstructural parcellation of cerebral cortex: a quantitative approach to cytoarchitectonics. Neuroimage. 9(1):165–177.
Schleicher A, Palomero-Gallagher N, Morosan P, Eickhoff SB, Kowalski T, de Vos K, Amunts K, Zilles K. 2005. Quantitative architectural analysis: a new approach to cortical mapping. Anat Embryol (Berl). 210(5–6):373–386.
Schleicher A, Zilles K. 1990. A quantitative approach to cytoarchitectonics: analysis of structural inhomogeneities in nervous tissue using an image analyser. J Microsc. 157:367–381.
Schleicher A, Amunts K, Geyer S, Kowalski T, Schormann T, Palomero-Gallagher N, Zilles K. 2000. A stereological approach to human cortical architecture: identification and delineation of cortical areas. J Chem Neuroanat. 20:31–47.
Schleicher A, Morosan P, Amunts K, Zilles K. 2009. Quantitative architectural analysis: a new approach to cortical mapping. J Autism Dev Disord. 39(11):1568–1581.
Schluppeck D, Curtis CE, Glimcher PW, Heeger DJ. 2006. Sustained activity in topographic areas of human posterior parietal cortex during memory-guided saccades. J Neurosci. 26(19):5098–5108.
Schluppeck D, Glimcher P, Heeger DJ. 2005. Topographic organization for delayed saccades in human posterior parietal cortex. J Neurophysiol. 94(2):1372–1384.
Seltzer B, Pandya DN. 1980. Converging visual and somatic sensory cortical input to the intraparietal sulcus of the rhesus monkey. Brain Res. 192(2):339–351.
Seltzer B, Pandya DN. 1986. Posterior parietal projections to the intraparietal sulcus of the rhesus monkey. Exp Brain Res. 62 (3):459–469.
Shulman GL, Ollinger JM, Akbudak E, Conturo TE, Snyder AZ, Petersen SE, Corbetta M. 1999. Areas involved in encoding and applying directional expectations to moving objects. J Neurosci. 19(21):9480–9496.
Silver MA, Kastner S. 2009. Topographic maps in human frontal and parietal cortex. Trends Cogn Sci. 13(11):488–495.
Silver MA, Ress D, Heeger DJ. 2005. Topographic maps of visual spatial attention in human parietal cortex. J Neurophysiol. 94(2):1358–1371.
Sunaert S, van Hecke P, Marchal G, Orban GA. 1999. Motion-responsive regions of the human brain. Exp Brain Res. 127(4):355–370.
Swisher JD, Halko MA, Merabet LB, McMains SA, Somers DC. 2007. Visual topography of human intraparietal sulcus. J Neurosci. 27(20):5326–5337.
Tsao DY, Vanduffel W, Sasaki Y, Fize D, Knutsen TA, Mandeville JB, Wald LL, Dale AM, Rosen BR, van Essen DC, et al. 2003. Stereopsis activates V3A and caudal intraparietal areas in Macaques and humans. Neuron. 39(3):555–568.
Turkeltaub PE, Eden GF, Jones KM, Zeffiro TA. 2002. Meta-analysis of the functional neuroanatomy of single-word reading. Neuroimage. 16(3):765–780.
Turkeltaub PE, Eickhoff SB, Laird AR, Fox M, Wiener M, Fox P. 2012. Minimizing within-experiment and within-group

effects in Activation Likelihood Estimation meta-analyses. Hum Brain Mapp. 33(1):1–13.
Tzelepi A, Ioannides AA, Poghosyan V. 2001. Early (N70m) neuromagnetic signal topography and striate and extrastriate generators following pattern onset quadrant stimulation. Neuroimage. 13(4):702–718.
Uddin LQ, Supekar K, Amin H, Rykhlevskaia E, Nguyen DA, Greicius MD, Menon V. 2010. Dissociable connectivity within human angular gyrus and intraparietal sulcus: evidence from functional and structural connectivity. Cereb Cortex. 20(11):2636–2646.
Uncapher MR, Hutchinson JB, Wagner AD. 2011. Dissociable effects of top-down and bottom-up attention during episodic encoding. J Neurosci. 31(35):12613–12628.
Vanni S, Tanskanen T, Seppa M, Uutela K, Hari R. 2001. Coinciding early activation of the human primary visual cortex and anteromedial cuneus. Proc Natl Acad Sci USA. 98 (5):2776–2780.
von Economo C, Koskinas GN. 1925. Die Cytoarchitektonik der Hirnrinde des erwachsenen Menschen. Wien und Berlin: Verlag von Julius Springer.
Wang L, Mruczek REB, Arcaro MJ, Kastner S. 2015. Probabilistic maps of visual topography in human cortex. Cereb Cortex. 25(10):3911–3931.
Ward JH. 1963. Hierarchical grouping to optimize an objective function. J Am Stat Assoc. 58:236–244.
Welchman AE. 2016. The human brain in depth: how we see in 3D. Annu Rev Vis Sci. 2:345–376.
Wree A, Schleicher A, Zilles K. 1982. Estimation of volume fractions in nervous tissue with an image analyzer. J Neurosci Methods. 6:29–43.
Xu Y. 2008. Representing connected and disconnected shapes in human inferior intraparietal sulcus. Neuroimage. 40(4): 1849–1856.
Zilles K, Amunts K. 2010. Centenary of Brodmann's map—conception and fate. Nat Rev Neurosci. 11(2):139–145.
Zilles K, Palomero-Gallagher N. 2001. Cyto-, myelo-, and receptor architectonics of the human parietal cortex. Neuroimage. 14:8–20.
Zlatkina V, Petrides M. 2014. Morphological patterns of the intraparietal sulcus and the anterior intermediate parietal sulcus of Jensen in the human brain. Proc Biol Sci. 281(1797): 1–8.